

Supporting Information

Difluoromethyl-1,3,4-oxadiazoles are selective, mechanism-based, and essentially irreversible inhibitors of histone deacetylase 6

Beate König,^{1,2} Paris R. Watson,² Nina Reßing,¹ Abigail D. Cragin,² Linda Schäker-Hübner,¹ David W. Christianson^{*2} and Finn K. Hansen^{*1}

¹ Department of Pharmaceutical and Cell Biological Chemistry, Pharmaceutical Institute, University of Bonn, 53121 Bonn, Germany.

² Roy and Diana Vagelos Laboratories, Department of Chemistry, University of Pennsylvania, 231 South 34th Street, Philadelphia, Pennsylvania 19104-6323, United States.

Corresponding authors:

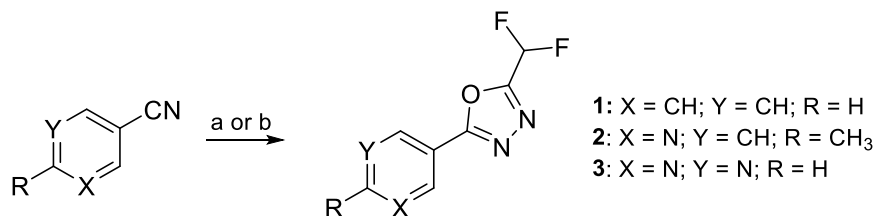
F.K.H.: E-mail, finn.hansen@uni-bonn.de

D.W.C: E-Mail: chris@sas.upenn.edu

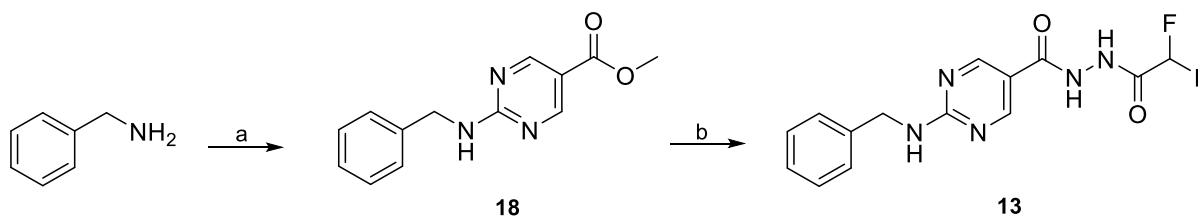
Content

1 Supplementary Schemes, Figures, Equations and Tables	S2
2 NMR Data of synthesized compounds	S10
3 HPLC Chromatograms	S39
4 References	S44

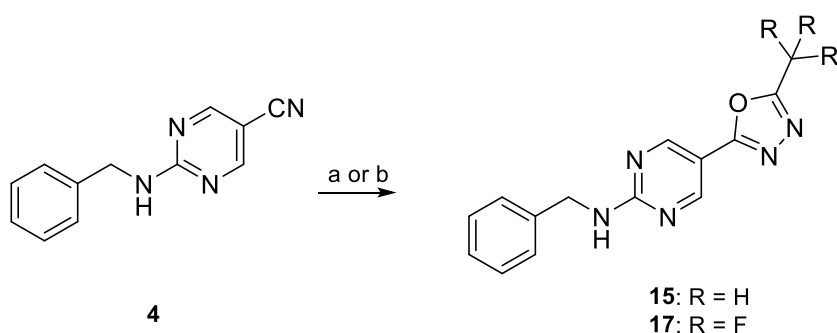
1 Supplementary Schemes, Figures, Equations and Tables



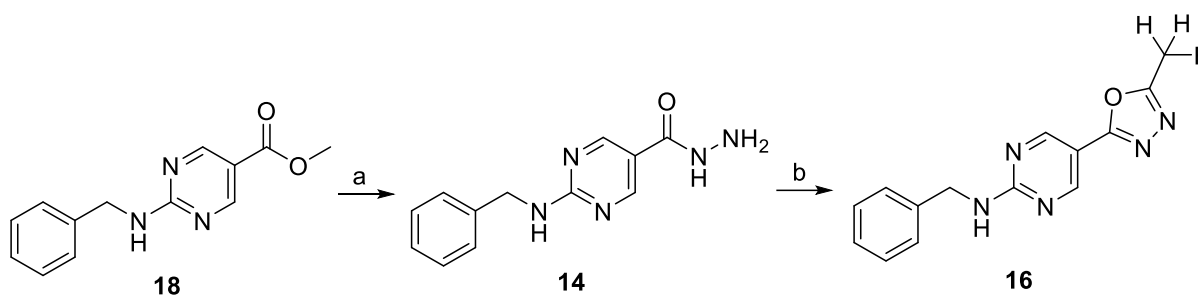
Scheme S1. Synthesis of HDAC6 inhibitor fragments. a) i: NaN₃, NH₄Cl, LiCl·H₂O, DMF, 100 °C, 150 W, 24 h; ii: DFAA, DCM, rt., 24 h (**1**, **3**); b) i: NaN₃, NH₄Cl, LiCl, DMF, 100 °C, 18 h; ii: difluoroacetic anhydride (DFAA), toluene, 70 °C, 18 h (**2**).



Scheme S2. Synthesis of the acylhydrazide **13**. a) Methyl 2-chlorpyrimidine-5-carboxylate, DIPEA, EtOH, 90 °C, 18 h; b) i: hydrazine monohydrate, MeOH, 70 °C, 3 h; ii: DFAA, DMF, 70 °C, 1 h.



Scheme S3. Synthesis of the trifluoromethyl-1,3,4-oxadiazole (**17**) and methyl-1,3,4-oxadiazole (**15**) analogs. a) i: NaN₃, NH₄Cl, LiCl, DMF, 100 °C, 18 h; ii: trifluoroacetic anhydride, toluene, 70 °C, 18 h (**14**); b) i: NaN₃, NH₄Cl, LiCl, DMF, 100 °C, 18 h; ii: acetic anhydride, toluene, 70 °C, 18 h; iii: K₂CO₃, MeOH/H₂O (**15**).



Scheme S4. Synthesis of hydrazide **14** and monofluoromethyl-1,3,4-oxadiazole **16**. a) hydrazine monohydrate, MeOH, 70 °C, 3 h; b) i: monofluoroacetic acid, DMF, 70 °C, 3 h; ii: Burgess reagent, THF, 60 °C, 18 h.

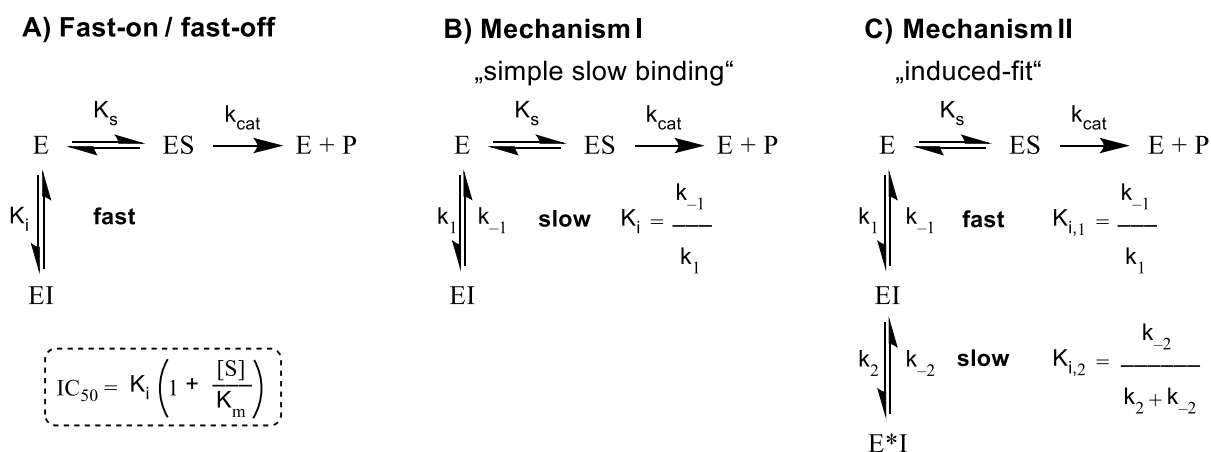


Figure S1. Representative examples of different kinetic mechanisms of enzyme inhibition, including the relationships between the respective association and dissociation rate constants (e. g., k_1 & k_{-1}) and the related equilibrium dissociation constant K_i . **A)** Fast-on/fast-off binding kinetics. For competitive fast-on/fast-off inhibitors the half maximum inhibitory concentration (IC_{50}) and the K_i are directly related by the Cheng-Prusoff equation¹; **B)** slow-binding Mechanism I: single-step slow binding, k_1 & k_{-1} are inherently slow; **C)** slow-binding Mechanism II: two-step slow binding. Initially, inhibitor and enzyme form an encounter complex [EI] that subsequently slowly undergoes isomerization to a binary enzyme inhibitor complex [E*I].²

HDAC6 Michaelis-Menten $K_M = 19.27 \mu\text{M}$

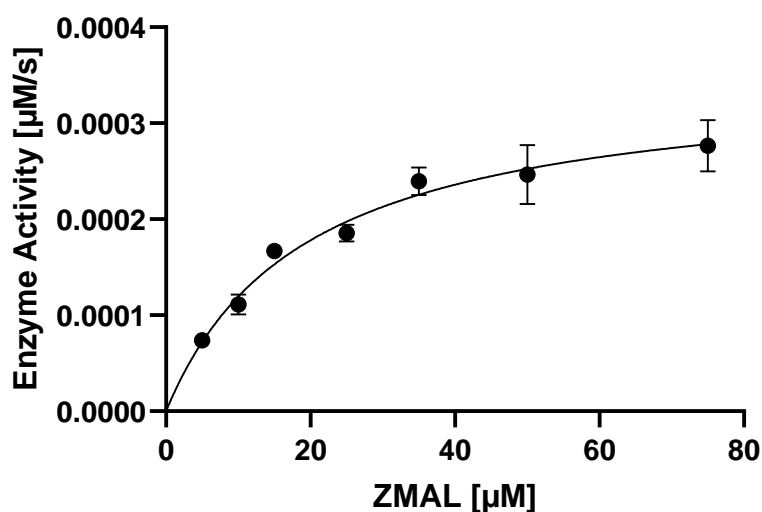


Figure S2. Michaelis-Menten constant K_M determination for HDAC6 using a series of substrate concentrations. Steady-state velocities [$\mu\text{M}\cdot\text{s}^{-1}$] (mean \pm SD) were plotted against the corresponding substrate concentrations [μM] and fitted to the Michaelis-Menten equation yielding the Michaelis-Menten constant: K_M HDAC6 = 19.27 μM . Experiment was performed in triplicates.

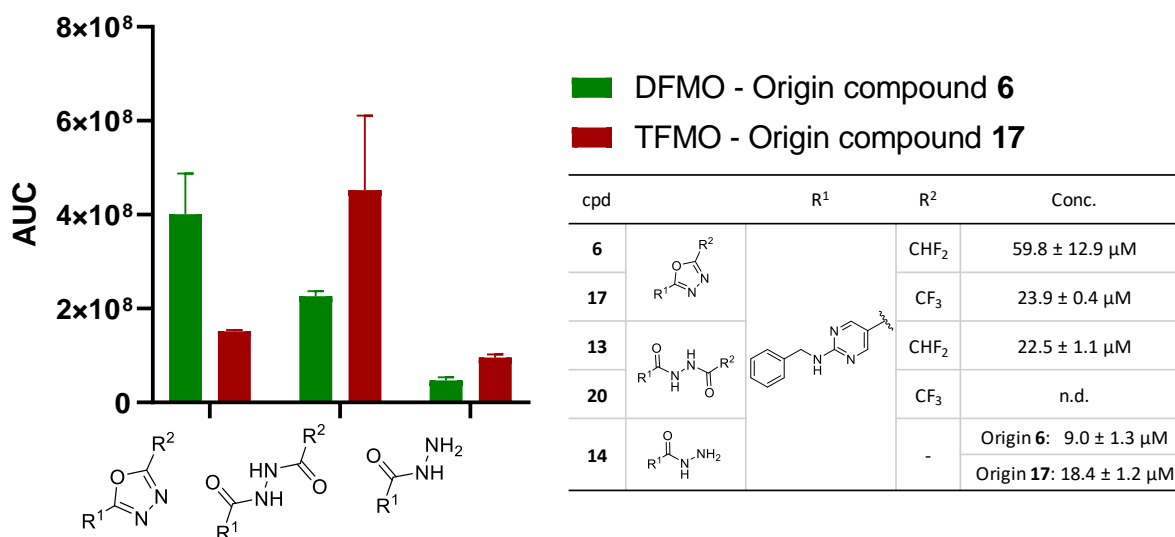


Figure S3. Quantified hydrolysis products from LC-UV-MS analysis after over night incubation of the respective compound (100 μM) with HDAC6. Experiments were performed in triplicates. DFMO: difluoromethyl-1,3,4-oxadiazole; TFMO: trifluoromethyl-1,3,4-oxadiazole. n.d.: not determined.

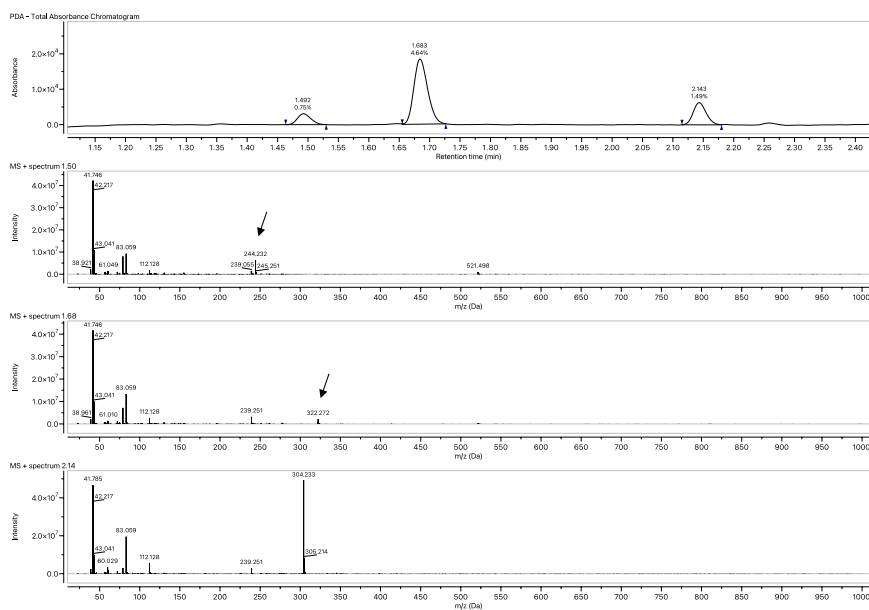
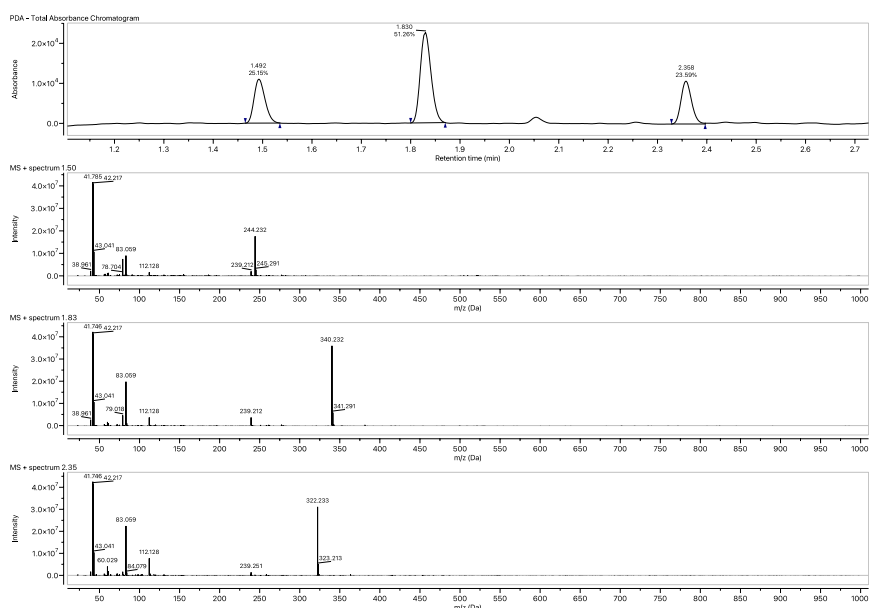
A**B**

Figure S4. Representative UV and related mass traces from two independent LC-UV-MS experiments. **A:** Compound **6** was incubated with HDAC6 overnight; **B:** Compound **17** was incubated with HDAC6 overnight; x axis: retention time in mins (chromatogram), m/z ration (mass spectras), y axis: intensity in Absorbance Units (AU). Experiments were performed in triplicates.

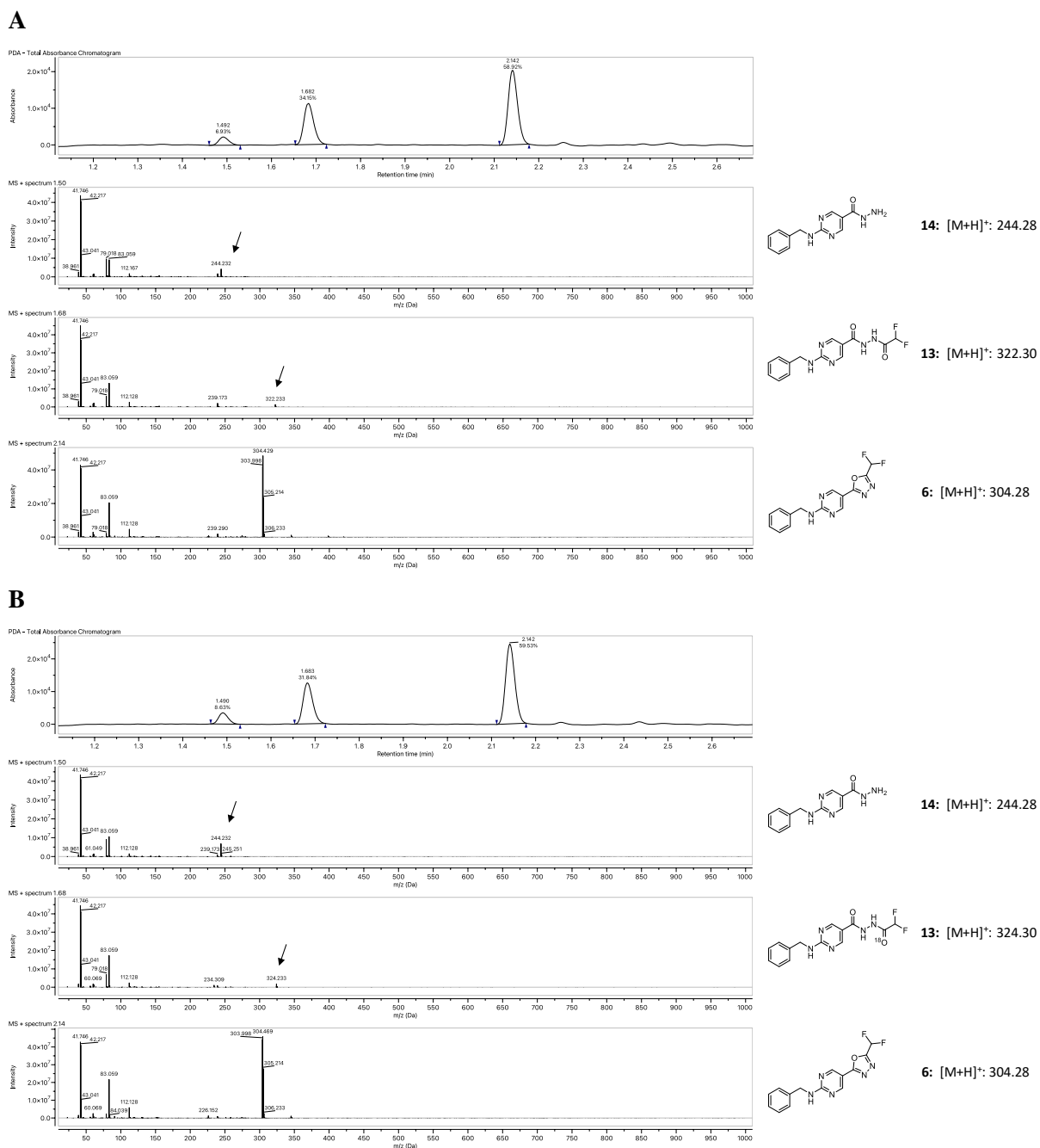


Figure S5. Representative UV and related mass traces of LC-UV-MS experiments. **A:** Compound **6** was incubated with HDAC6 overnight in $H_2^{16}O$ water; **B:** Compound **6** incubated with HDAC6 overnight in $H_2^{18}O$ water; x axis: retention time in mins (chromatogram), m/z ratio (mass spectras), y axis: intensity in Absorbance Units (AU). Experiments were performed in triplicates.

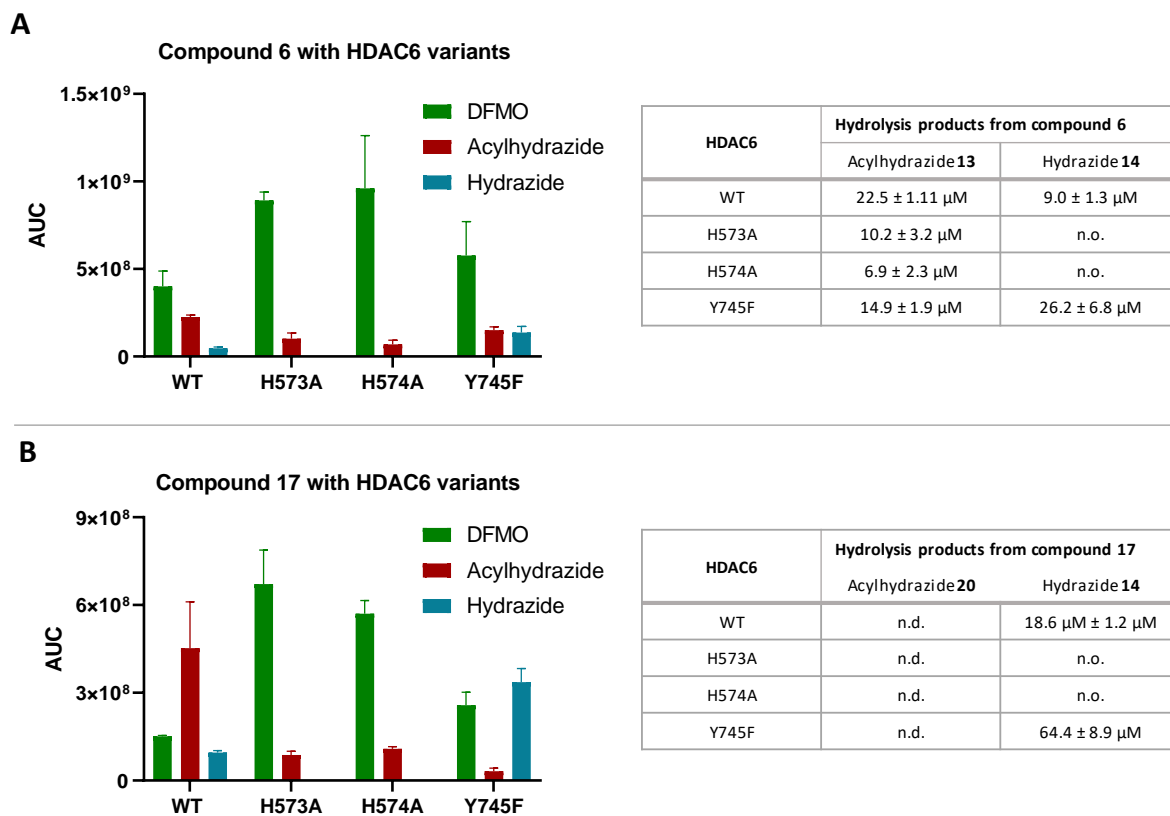


Figure S6. Quantified hydrolysis products from LC-UV-MS analysis after over night incubation of the respective compound (100 μM) with various HDAC6 mutants (wild-type (WT), H573A, H574A, Y745F). Experiments were performed in triplicates. n.d.: not determined; n.o.: not observed.

$$[P] = v_{ss}t + \frac{v_{in}-v_{ss}}{k_{obs}}(1 - e^{-k_{obs}t}) \quad (\text{Eq. 1})$$

Equation 1. Time-dependent product formation for inhibitors showing slow-binding Mechanism I&II. [P]: amount of generated AMC; v_{ss} : steady-state velocity (product formation); t: time; v_{in} : initial velocity (product formation); k_{obs} : apparent first-order rate constant for the conversion from v_{in} to v_{ss} .

$$k_{obs} = k_{-1} + k_1 \left(1 + \frac{[S]}{K_M}\right) [I] \quad (\text{Eq. 2})$$

Equation 2. The single-step slow-binding Mechanism I results in a linear relationship between k_{obs} and inhibitor concentration. k_{-1} : dissociation rate constant; k_1 : association rate constant; [S]: substrate concentration; K_M : Michelis-Menten constant; [I]: inhibitor concentration.

$$k_{obs} = k_{-2} + \frac{k_2}{[I] + K_{i,1} \left(1 + \frac{[S]}{K_M}\right)} [I] \quad (\text{Eq. 3})$$

Equation 3. The two-step slow-binding Mechanism II results in a hyperbolic relationship between k_{obs} and inhibitor concentration. k_{-2} : secondary dissociation rate constant; k_2 : secondary association rate constant; $K_{i,1}$: equilibrium dissociation constant of the enzyme inhibitor encounter complex [EI].

Table S1: Data collection and refinement statistics^a

HDAC6 CD2–13 Complex	
Space group	<i>P</i> 2 ₁ 2 ₁ 2 ₁
a,b,c (Å)	74.60, 92.30, 96.60
α, β, γ (°)	90.00, 90.00, 90.00
R _{merge} ^b	0.210 (0.706)
R _{pim} ^c	0.084(0.289)
CC _{1/2} ^d	0.993(0.851)
Redundancy	1.9
Completeness (%)	99.5(94.3)
I/σ	7.3(2.5)
Refinement	
Resolution (Å)	36.216–2.00 (2.07–2.00)
No. reflections	90179 (8857)
R _{work} /R _{free} ^e	0.185/0.223 (0.228/0.0.266)
Number of Atoms ^f	
Protein	5469
Ligand	52
Solvent	424
Average B factors (Å ²)	
Protein	15
Ligand	20
Solvent	20
RMS Deviations	
Bond lengths (Å)	0.03
Bond angles (°)	1.4
Ramachandran Plot ^g	
Favored	97.01
Allowed	2.99
Outliers	0.00

^aValues in parentheses refer to the highest-resolution shell of data.

^b $R_{\text{merge}} = \sum_h \sum_i |I_{i,h} - \langle I \rangle_h| / \sum_h \sum_i I_{i,h}$, where $\langle I \rangle_h$ is the average intensity calculated for reflection h from i replicate measurements.

^c $R_{\text{p.i.m.}} = (\sum_h (1/(N-1))^{1/2} \sum_i |I_{i,h} - \langle I \rangle_h|) / \sum_h \sum_i I_{i,h}$, where N is the number of reflections and $\langle I \rangle_h$ is the average intensity calculated for reflection h from replicate measurements.

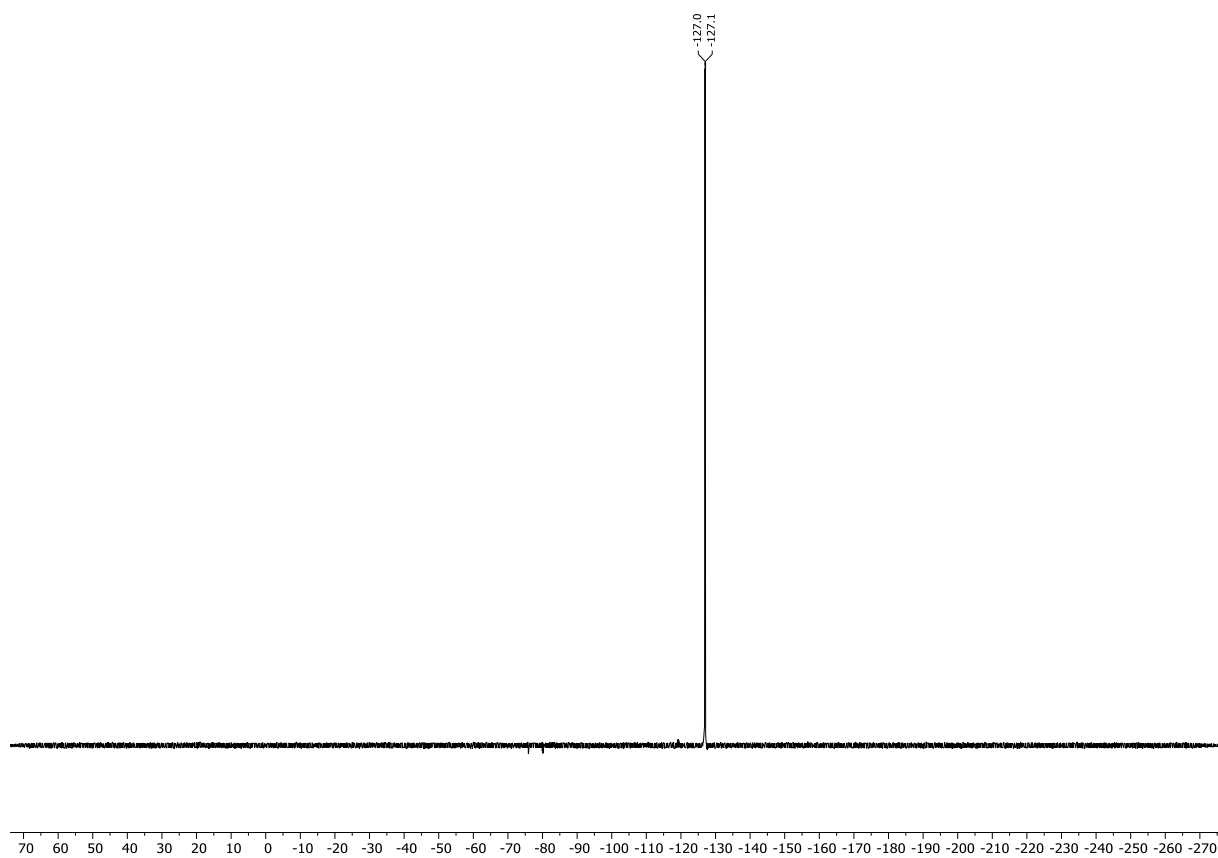
^dPearson correlation coefficient between random half-datasets.

^e $R_{\text{work}} = \sum ||F_o| - |F_c|| / \sum |F_o|$ for reflections contained in the working set. $|F_o|$ and $|F_c|$ are the observed and calculated structure factor amplitudes, respectively. R_{free} is calculated using the same expression for reflections contained in the test set held aside during refinement.

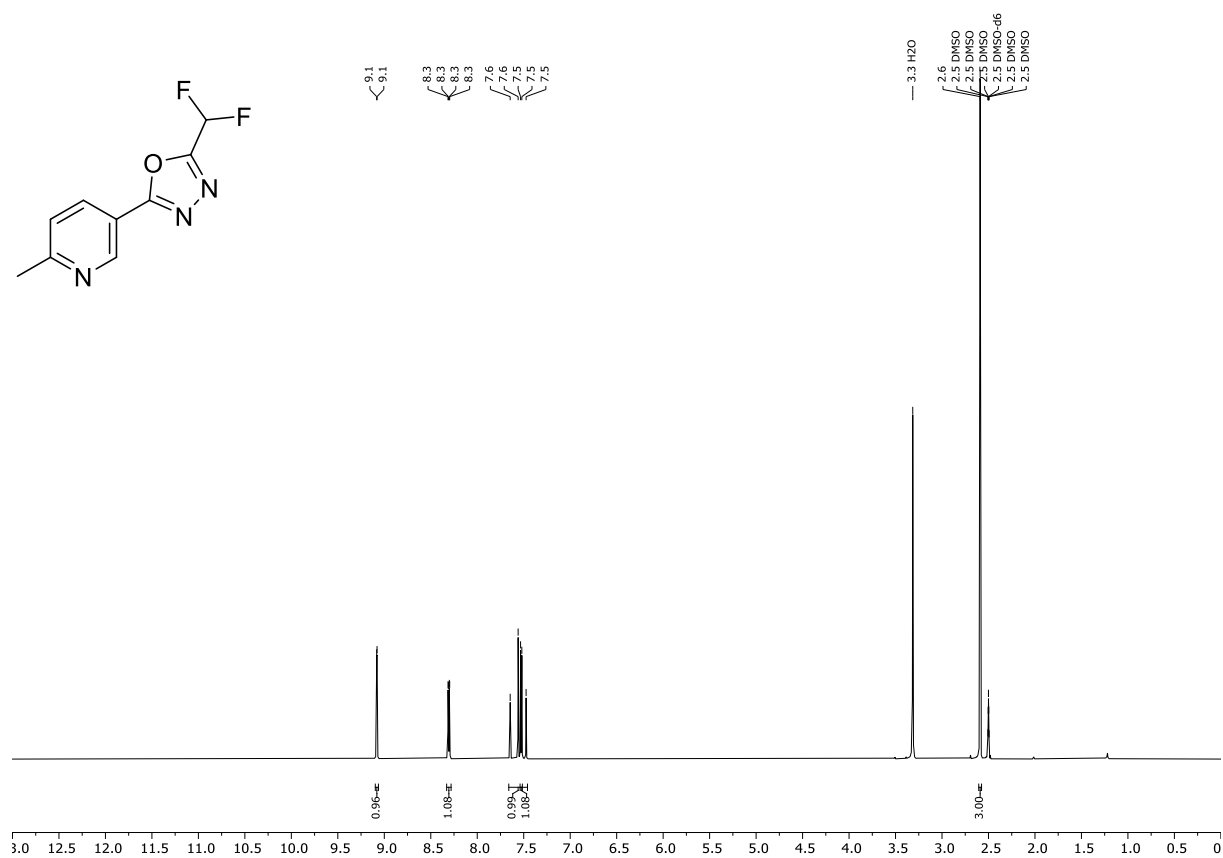
^fPer asymmetric unit.

^gCalculated with MolProbity.

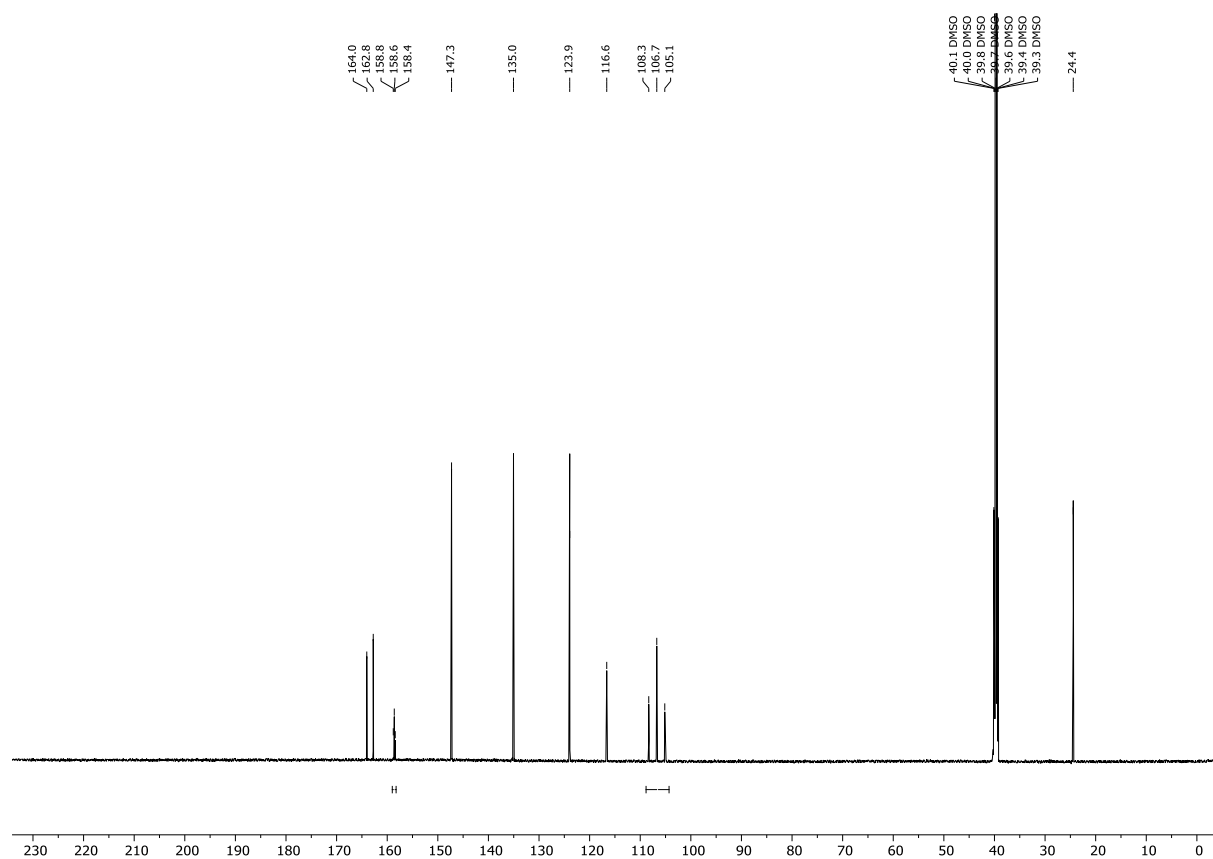
^{19}F NMR spectrum of **1 (377 MHz, CDCl_3)**



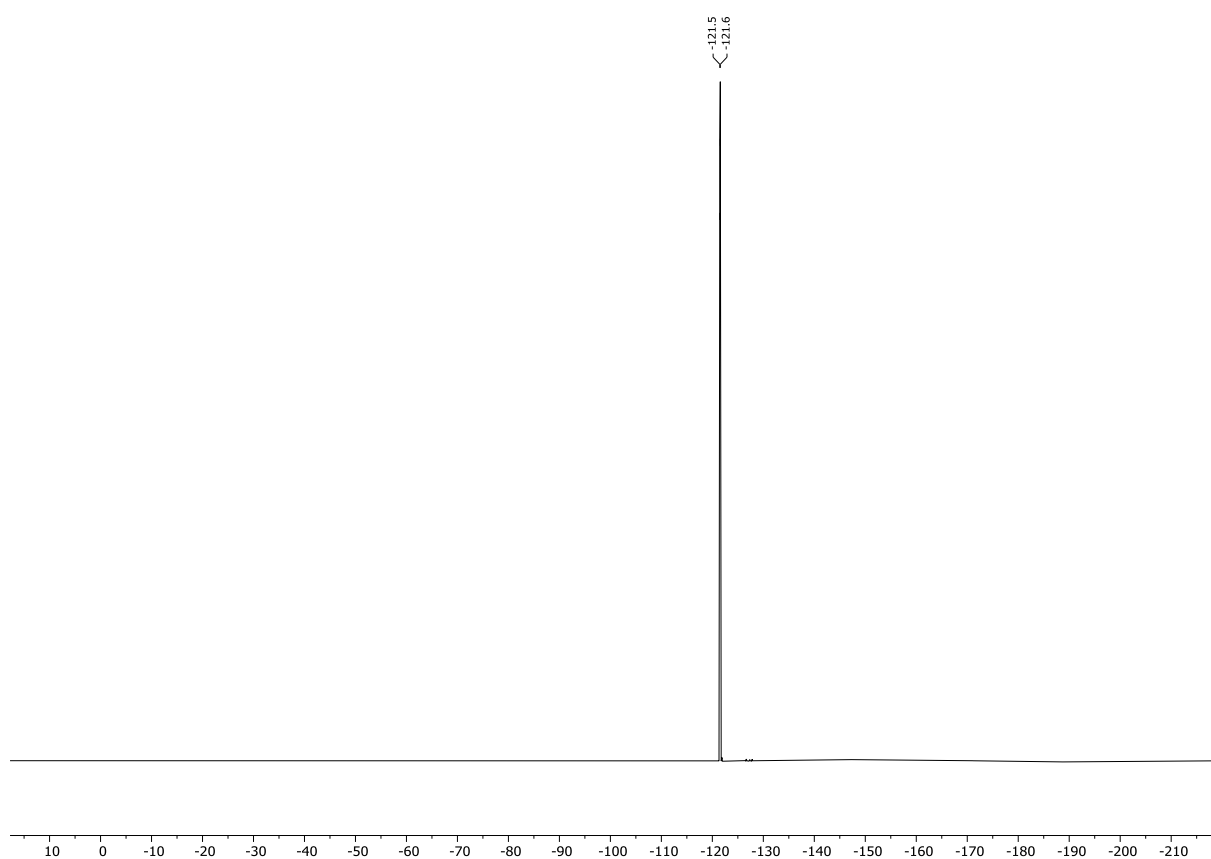
¹H NMR spectrum of 2 (600 MHz, DMSO-*d*₆)



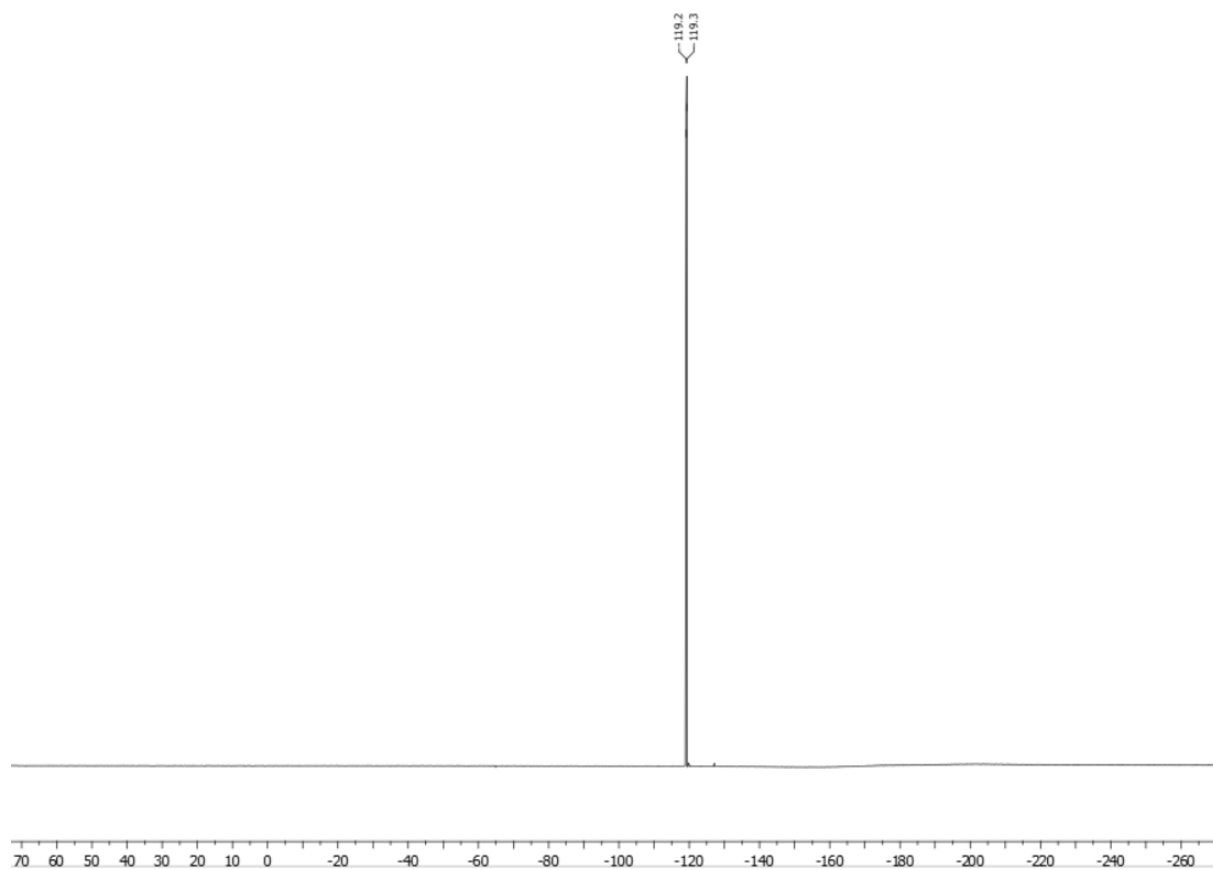
¹³C NMR spectrum of 2 (151 MHz, DMSO-*d*₆)



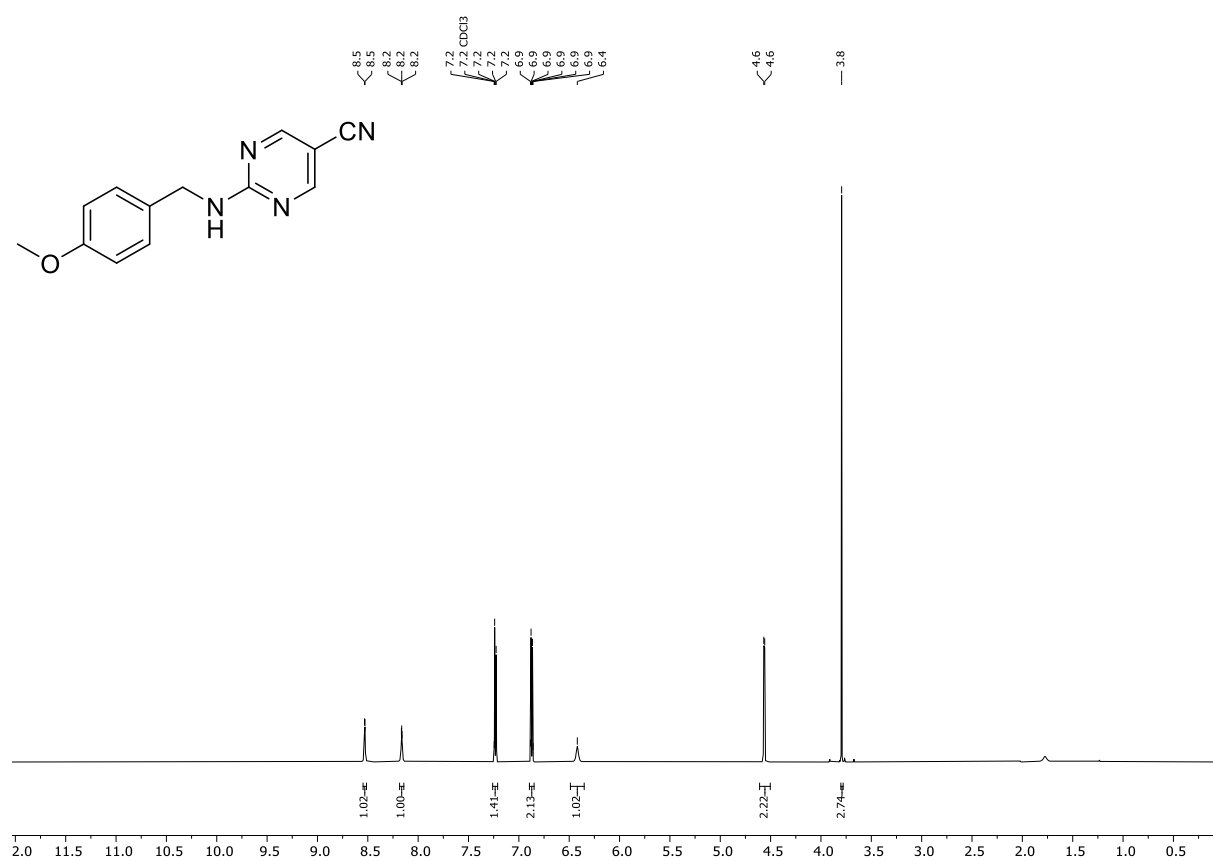
^{19}F NMR spectrum of **2** (565 MHz, DMSO- d_6)



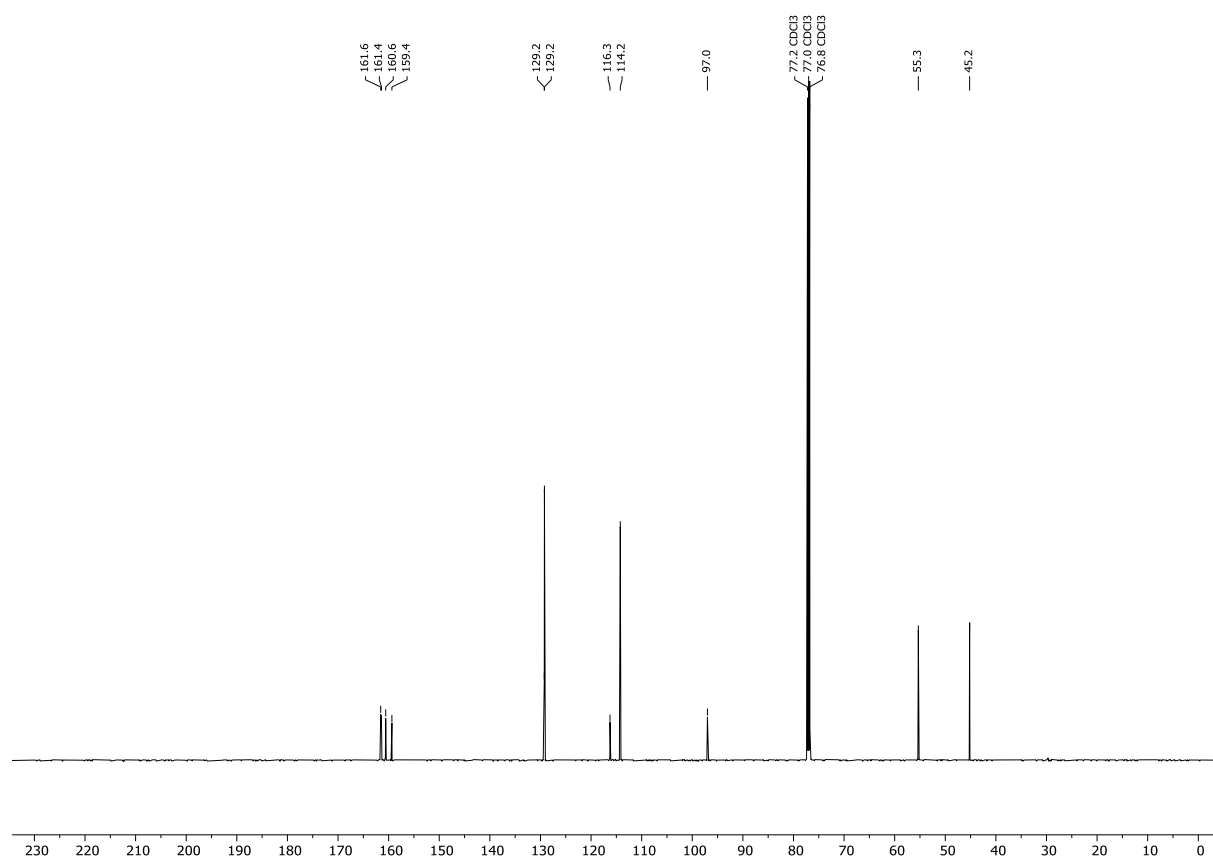
^{19}F NMR spectrum of **3** (377 MHz, CDCl_3)



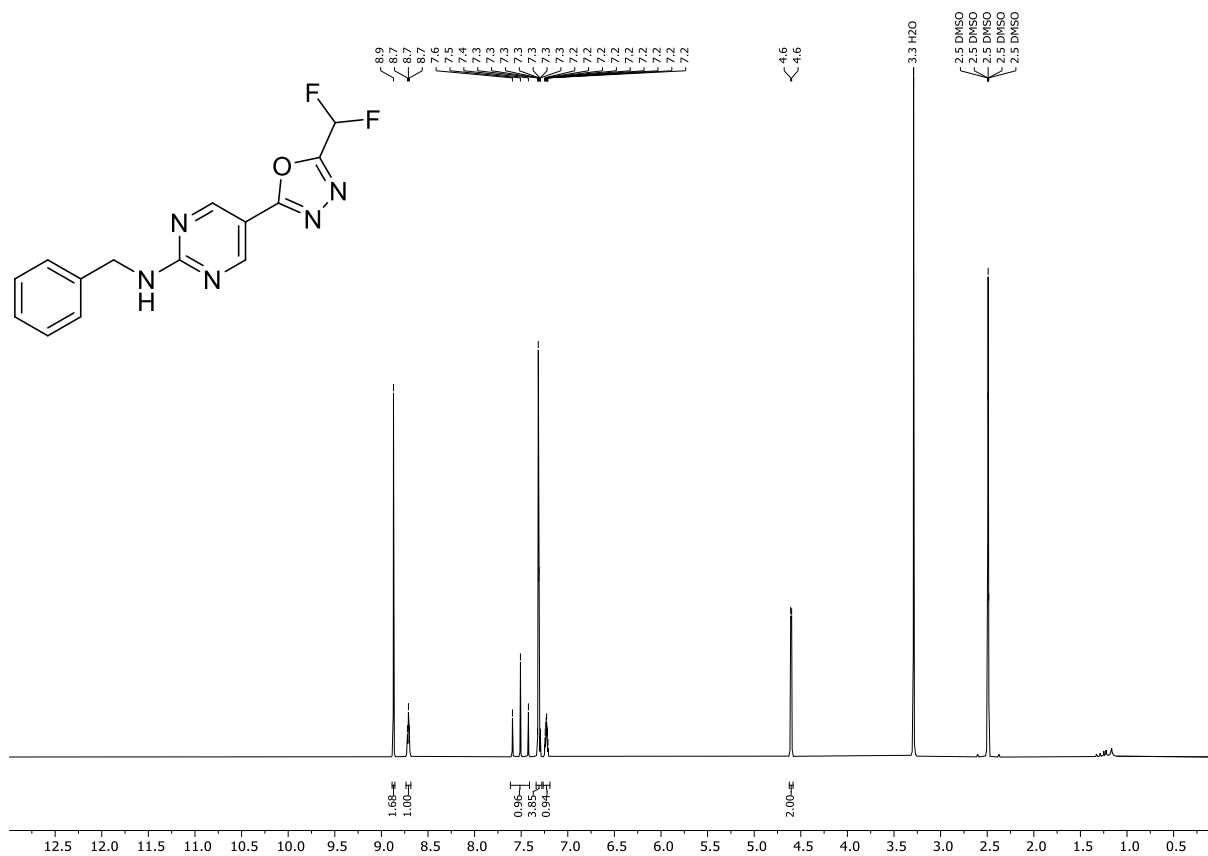
¹H NMR spectrum of 5 (600 MHz, CDCl₃)



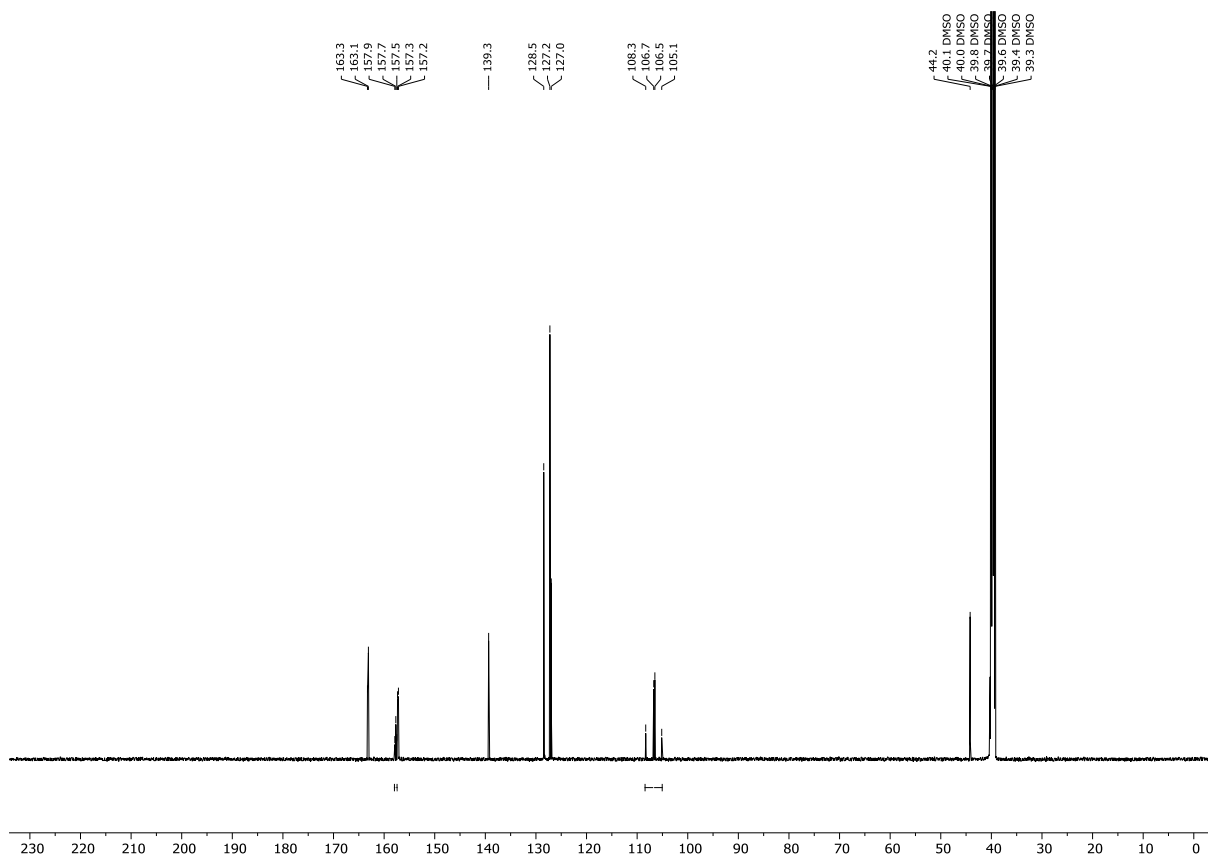
¹³C NMR spectrum of 5 (151 MHz, CDCl₃)



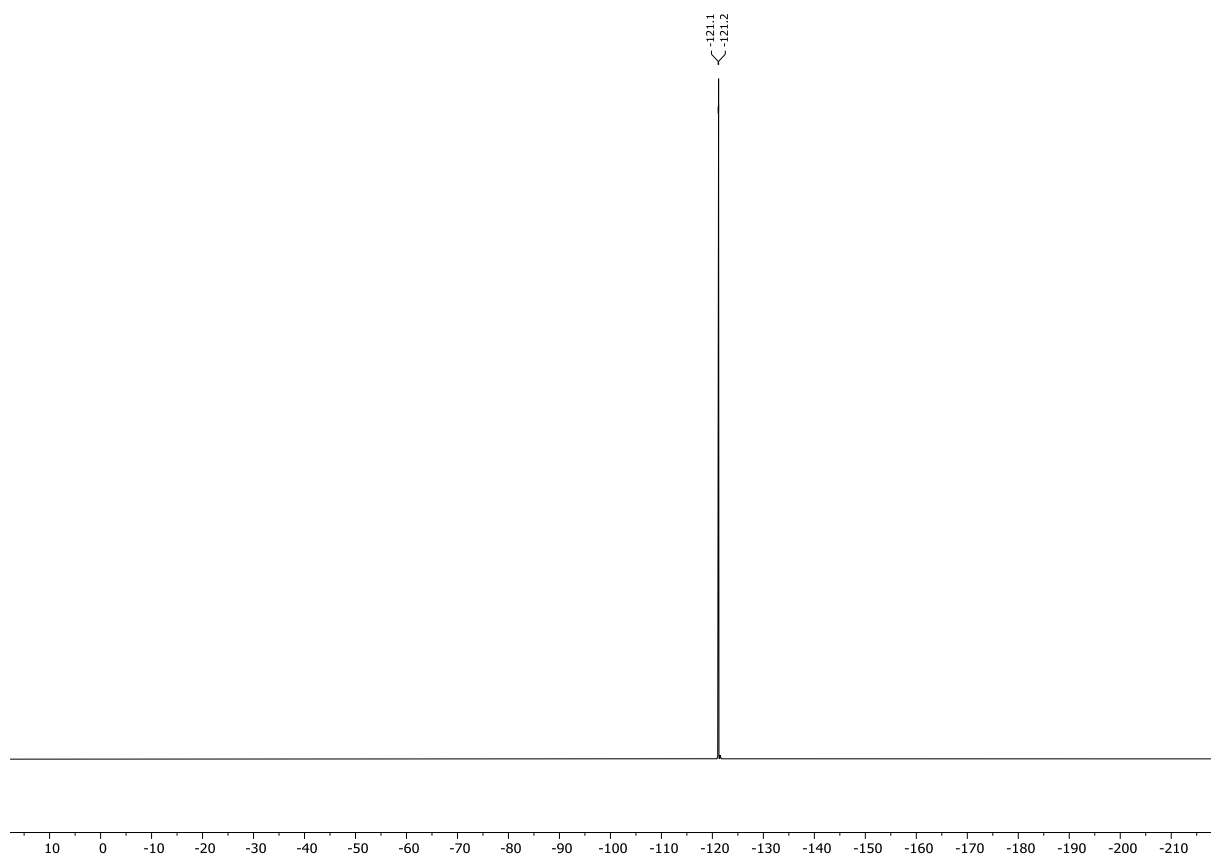
¹H NMR spectrum of **6** (600 MHz, DMSO-d₆)



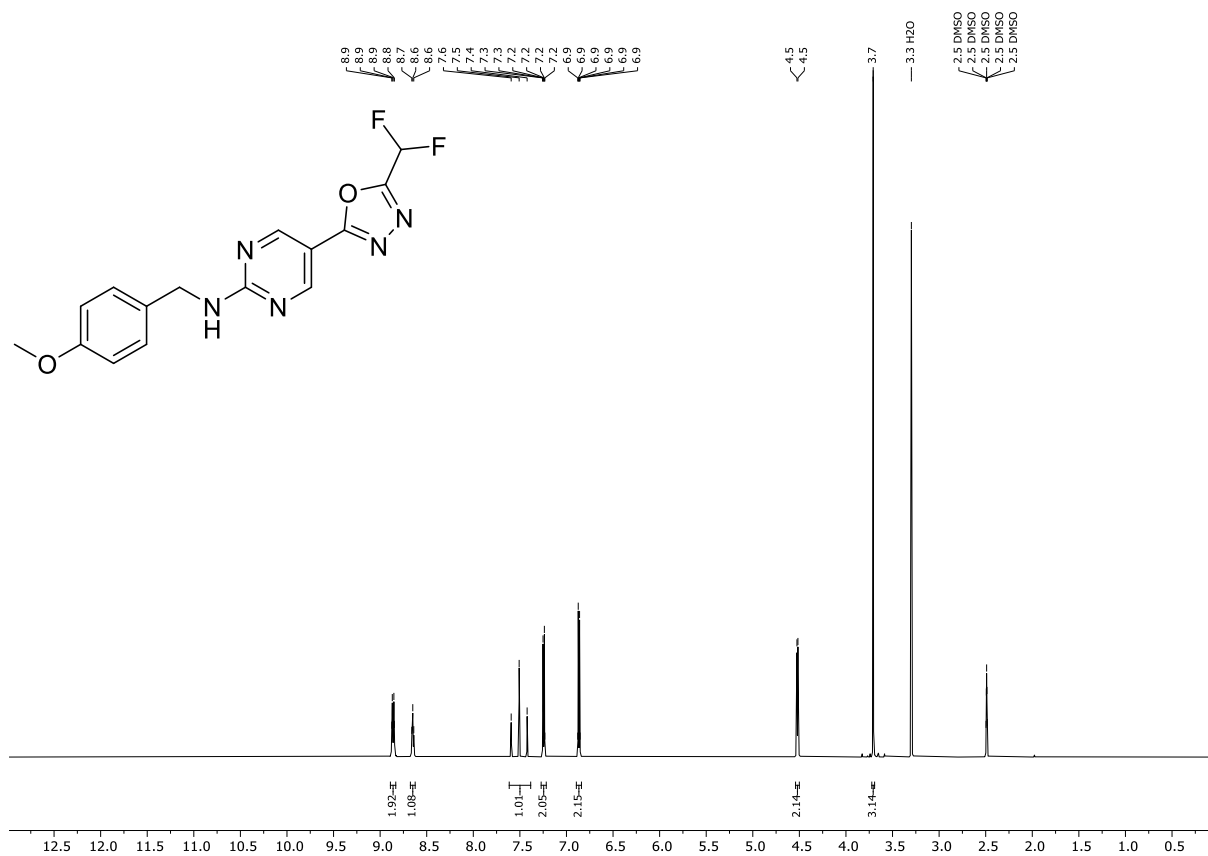
¹³C NMR spectrum of **6** (151 MHz, DMSO-d₆)



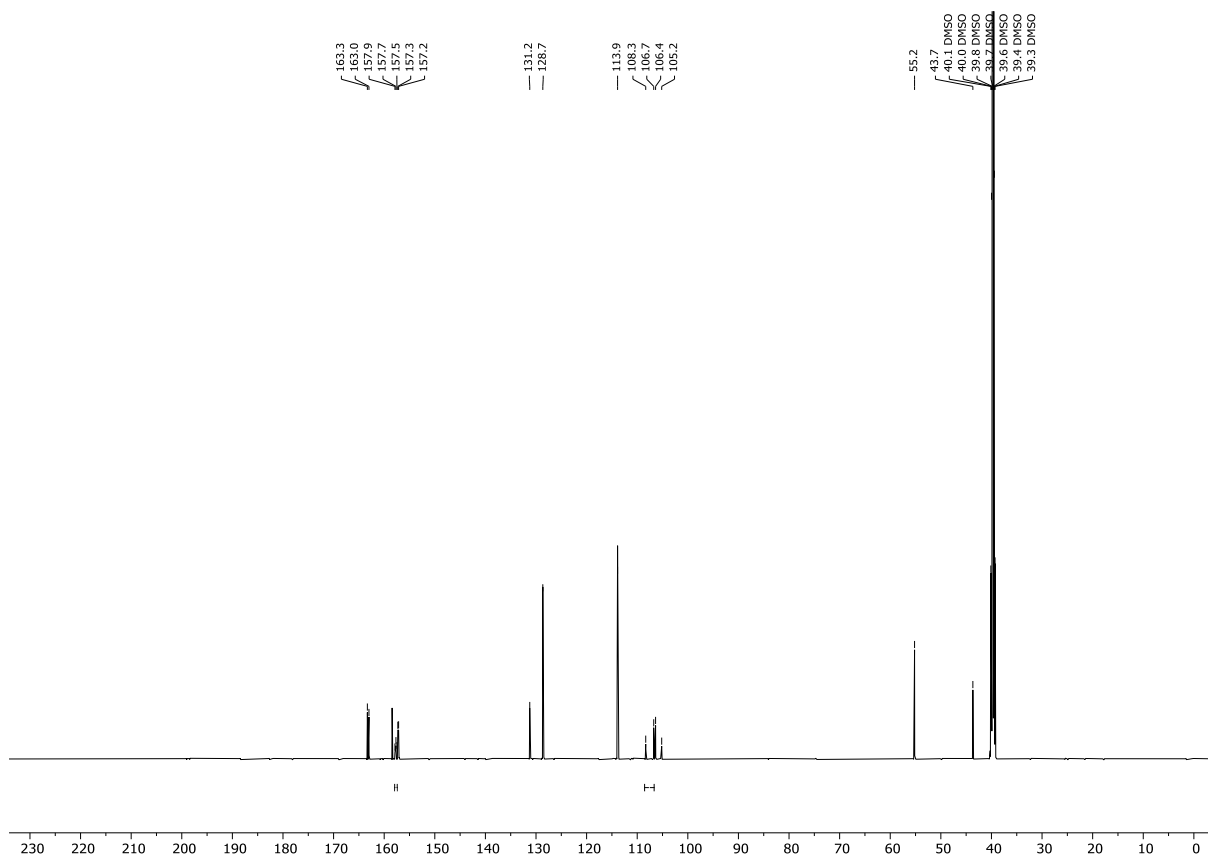
^{19}F NMR spectrum of **6** (565 MHz, $\text{DMSO-}d_6$)



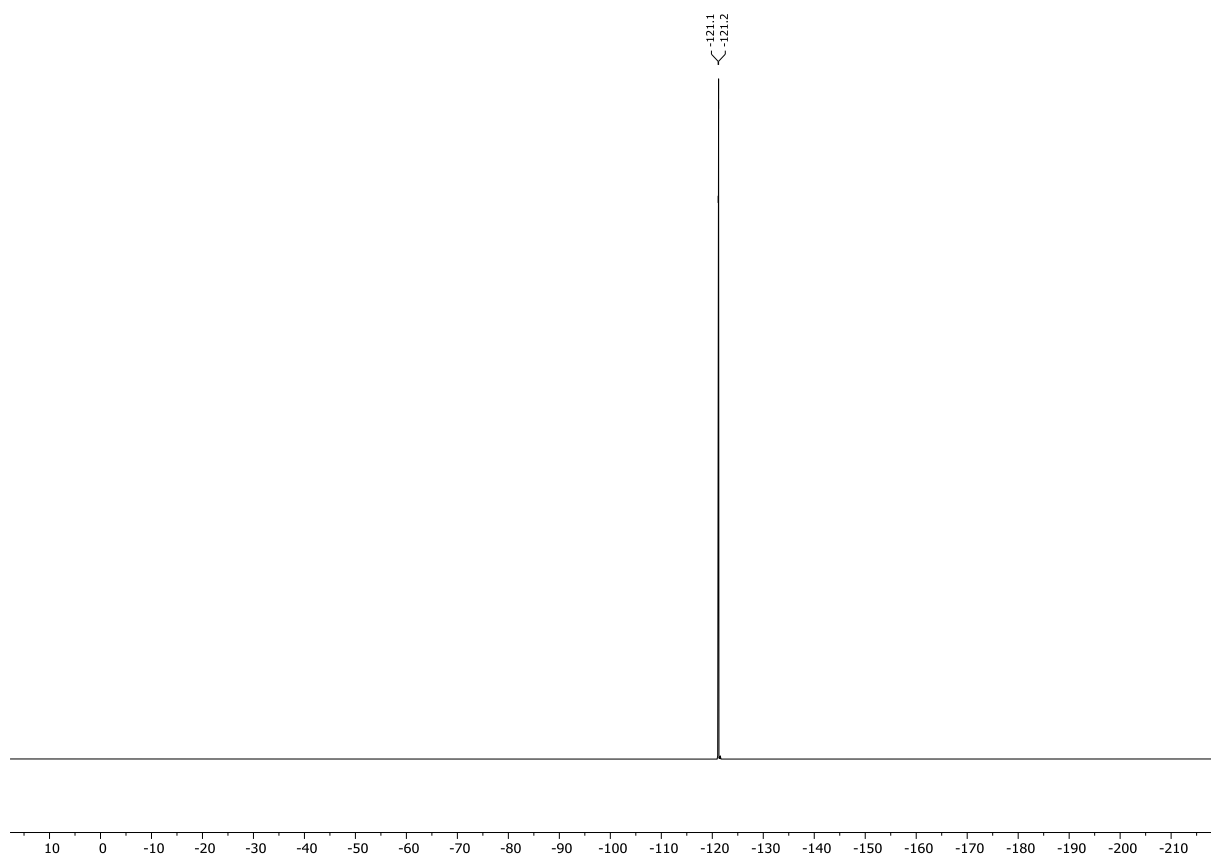
¹H NMR spectrum of 7 (600 MHz, DMSO-*d*₆)



¹³C NMR spectrum of 7 (151 MHz, DMSO-*d*₆)



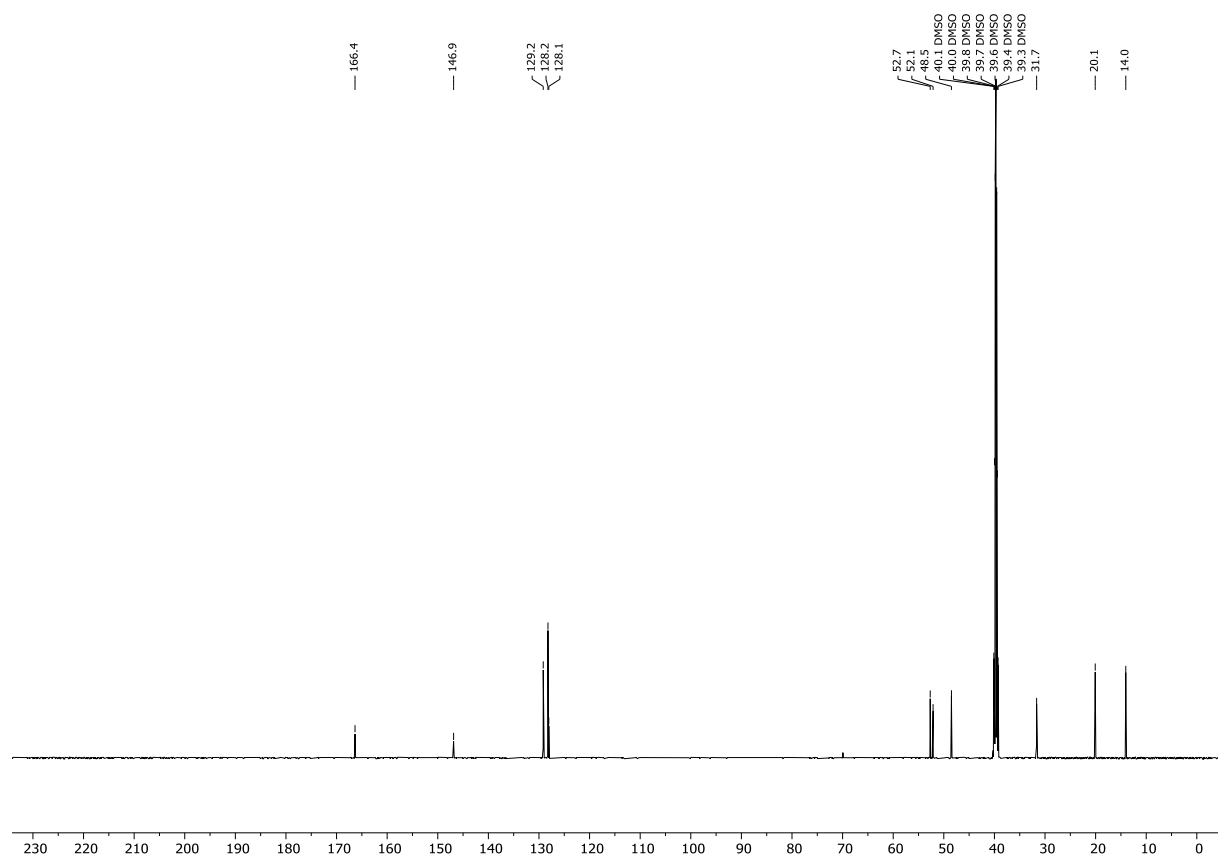
^{19}F NMR spectrum of **7** (565 MHz, $\text{DMSO-}d_6$)



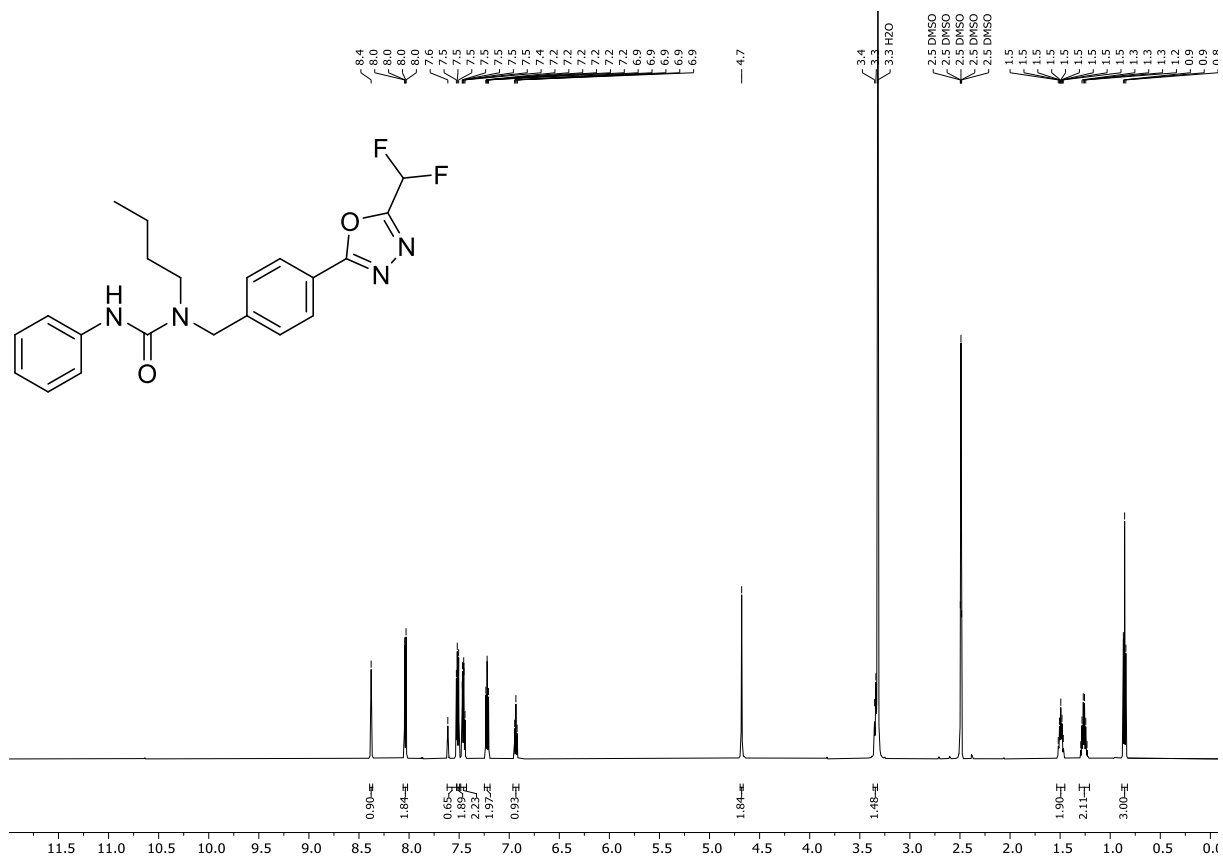
¹H NMR spectrum of 8 (600 MHz, DMSO-*d*₆)



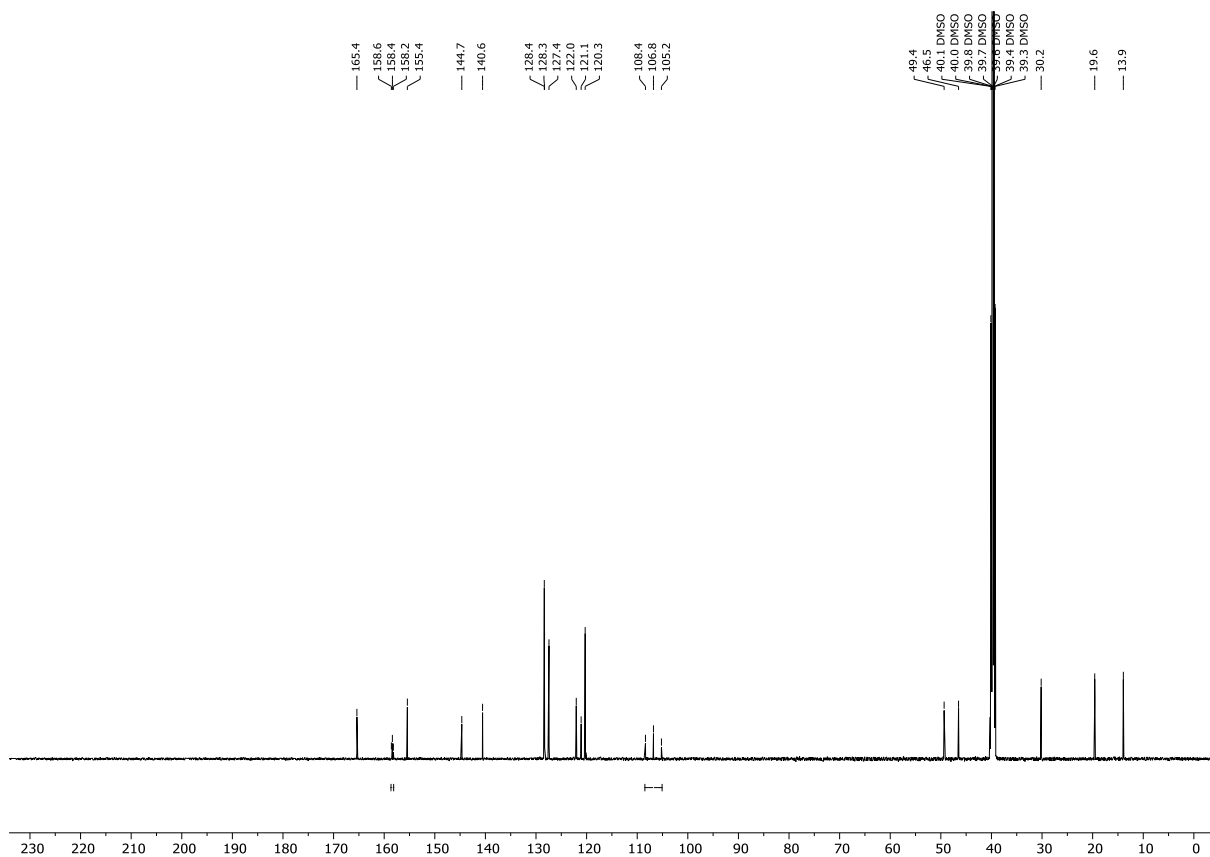
¹³C NMR spectrum of 8 (151 MHz, DMSO-*d*₆)



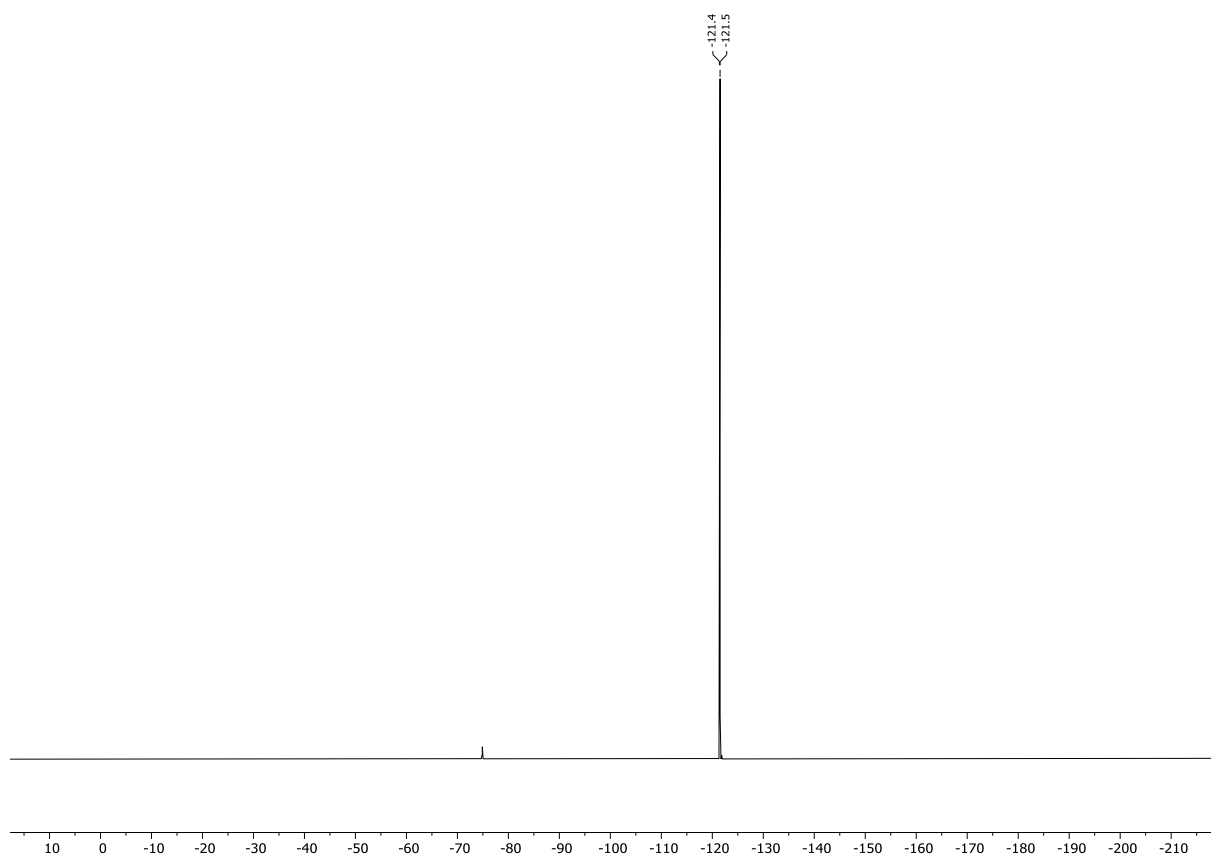
¹H NMR spectrum of 9 (600 MHz, DMSO-*d*₆)



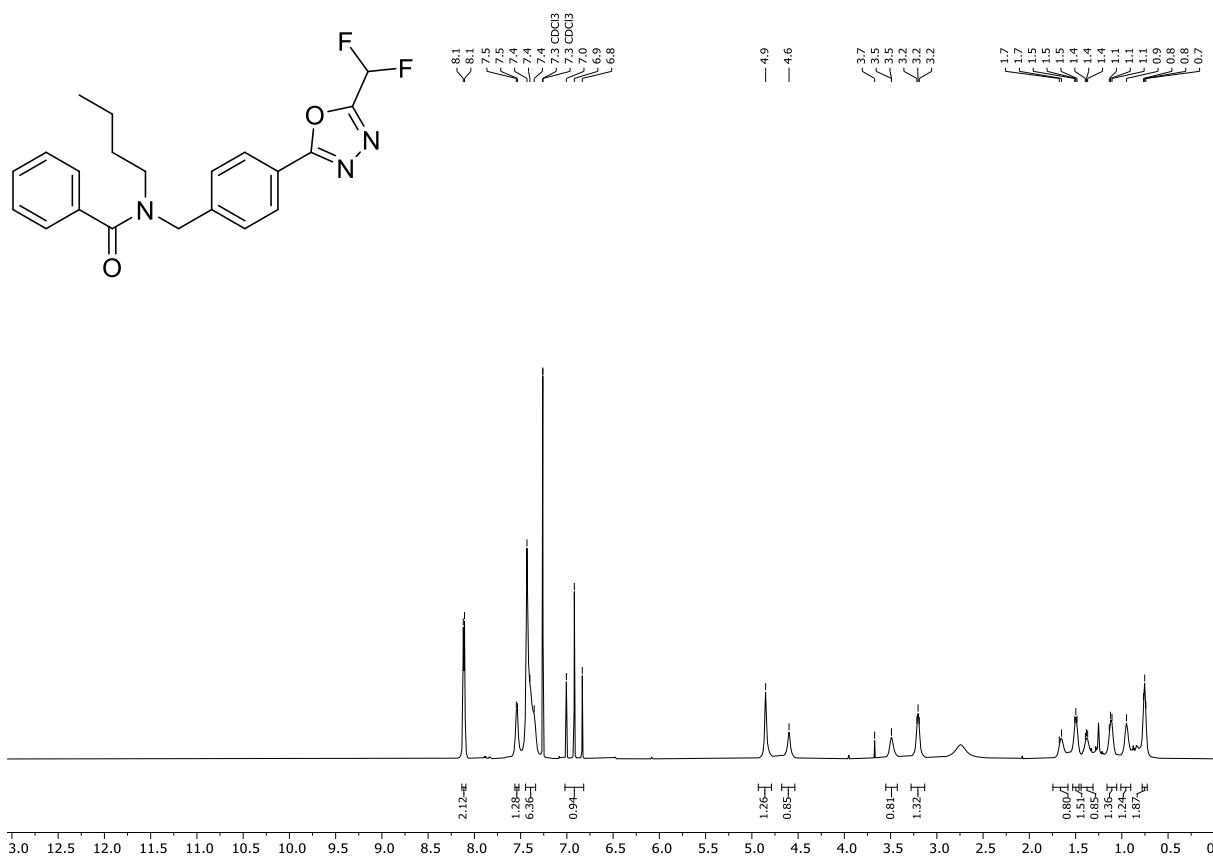
¹³C NMR spectrum of 9 (151 MHz, DMSO-*d*₆)



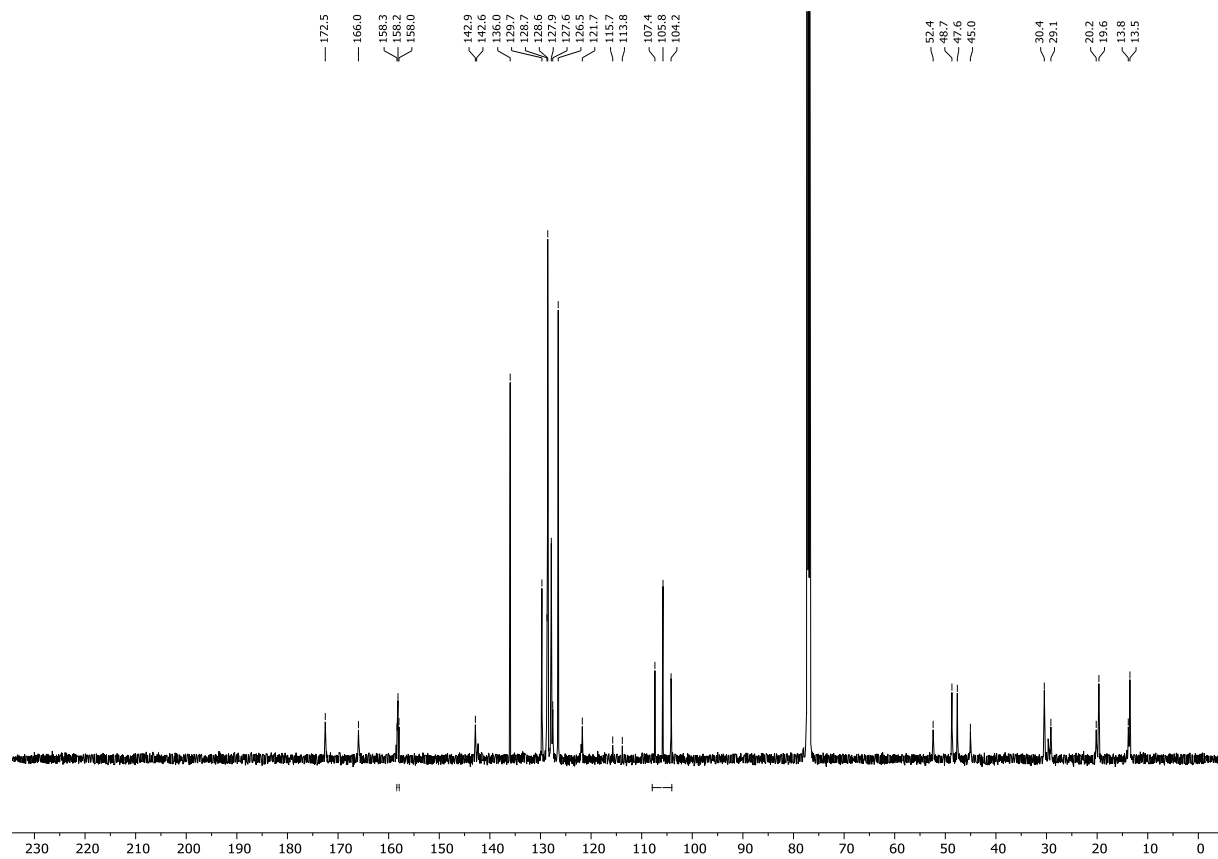
^{19}F NMR spectrum of **9** (565 MHz, DMSO- d_6)



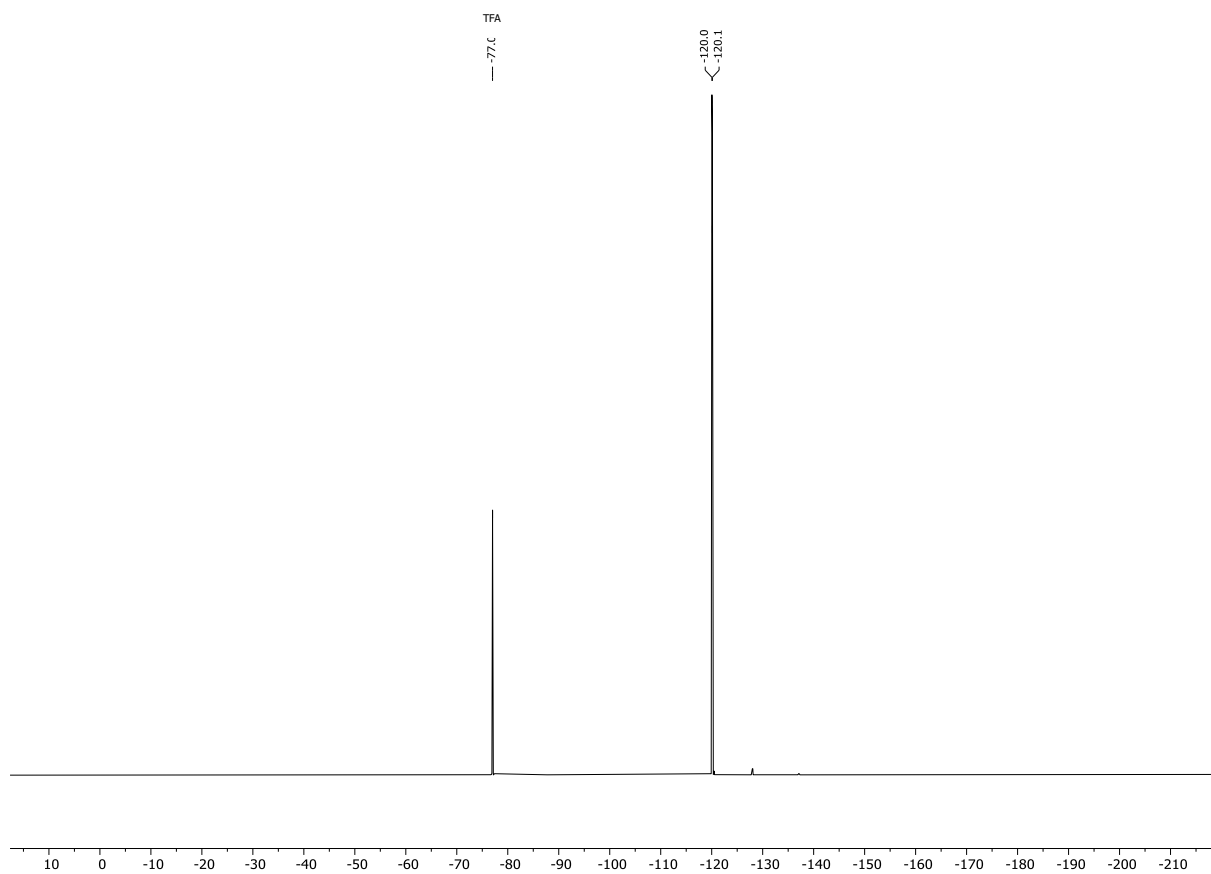
¹H NMR spectrum of 10 (600 MHz, CDCl₃)



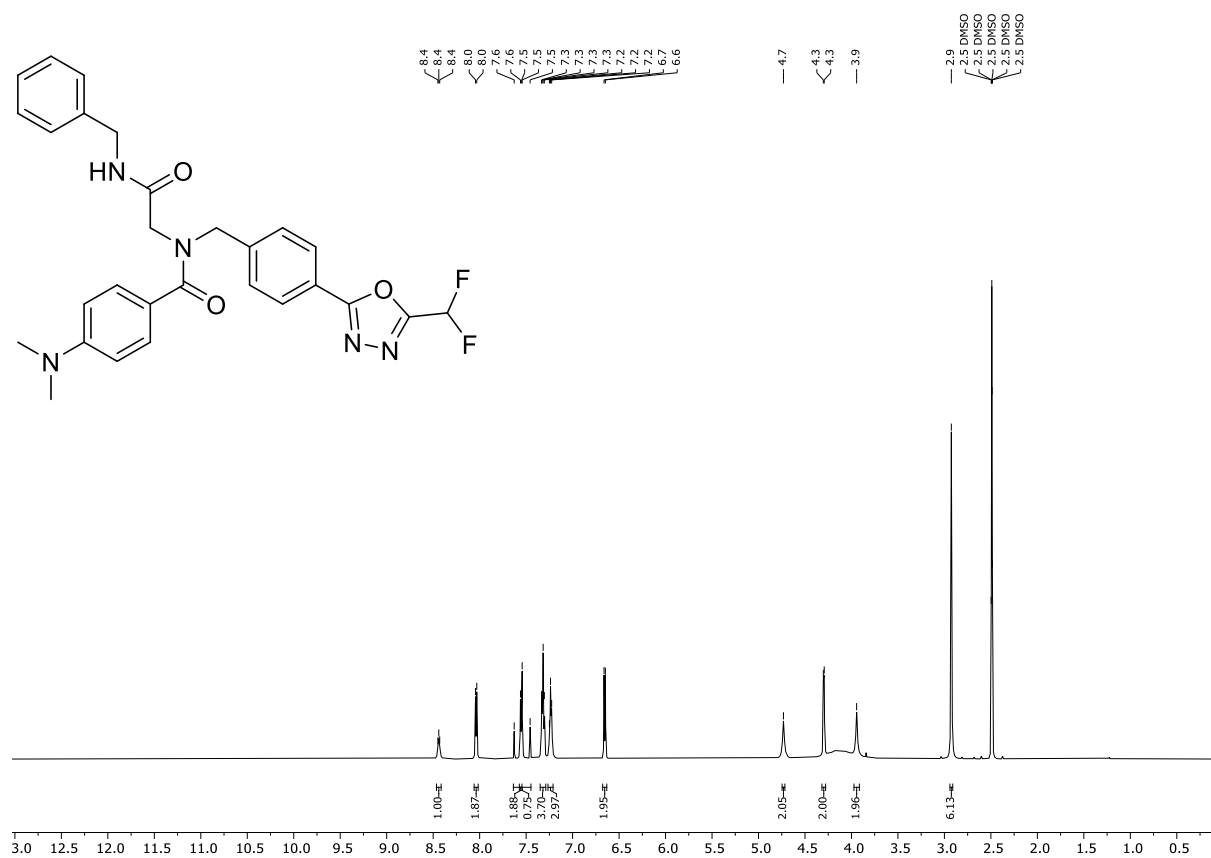
¹³C NMR spectrum of 10 (151 MHz, CDCl₃)



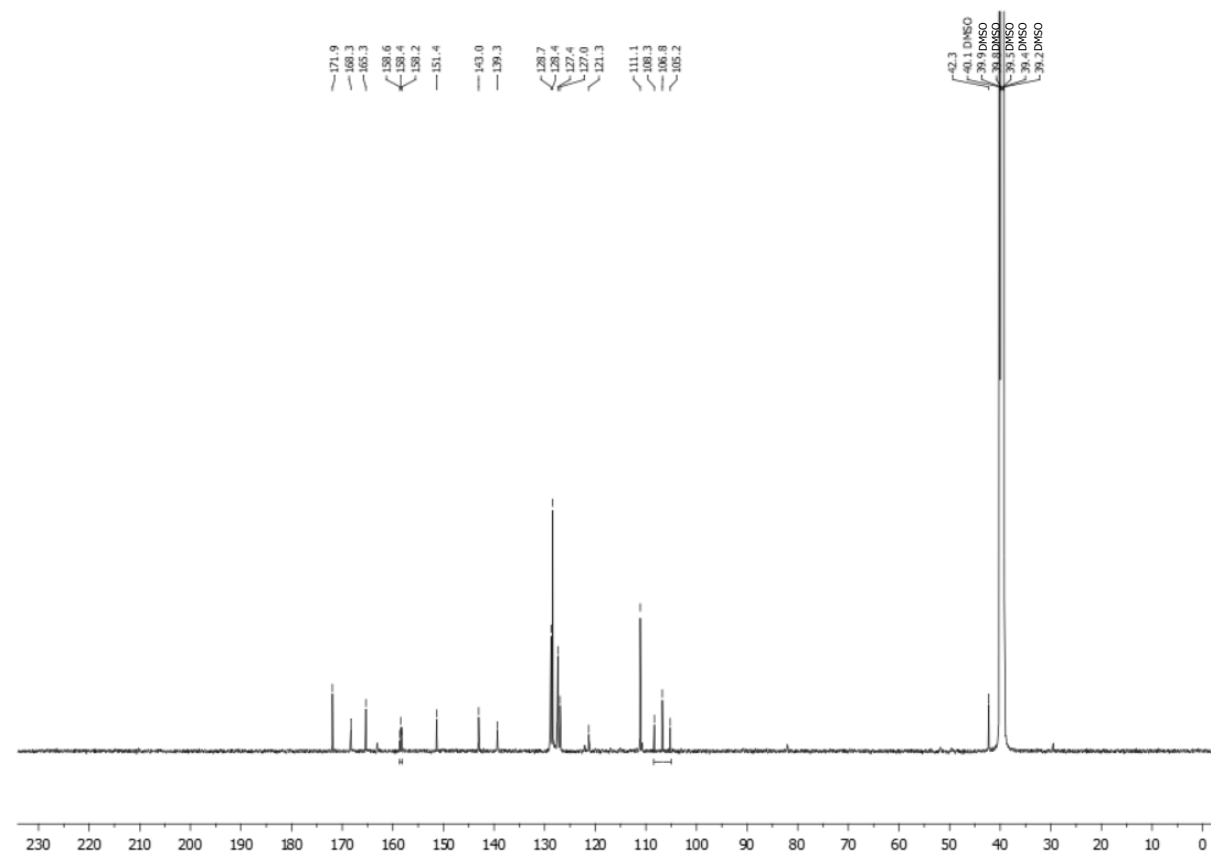
^{19}F NMR spectrum of **10 (565 MHz, CDCl_3)**



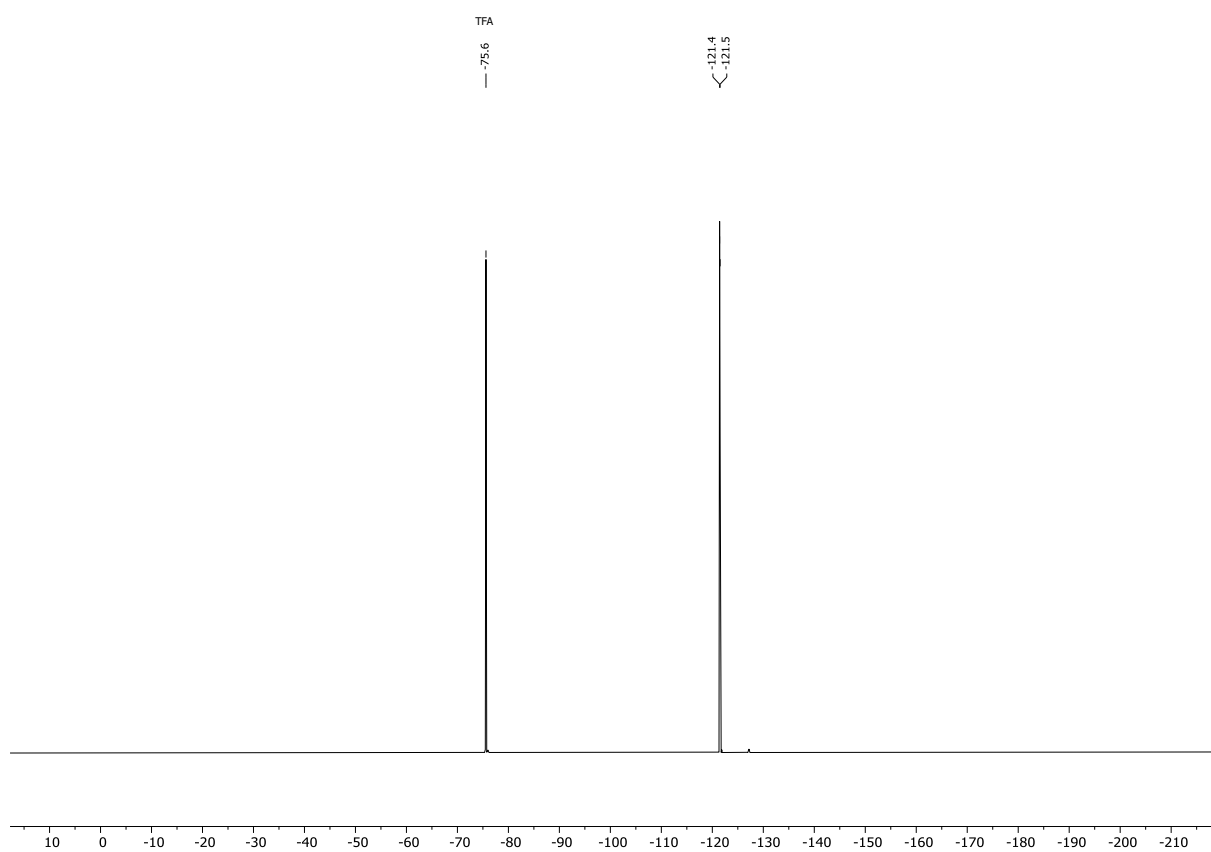
¹H NMR spectrum of 12 (600 MHz, DMSO-*d*₆)



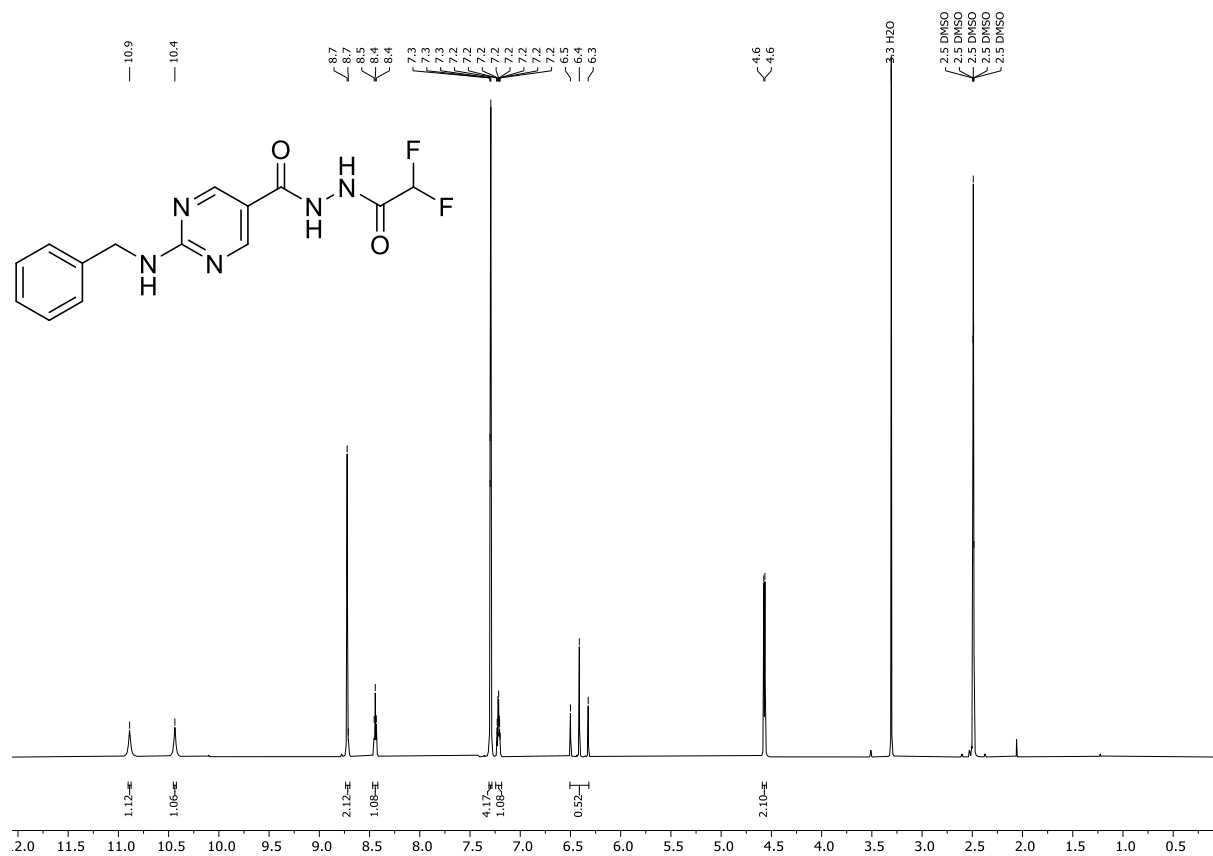
¹³C NMR spectrum of 12 (151 MHz, DMSO-*d*₆)



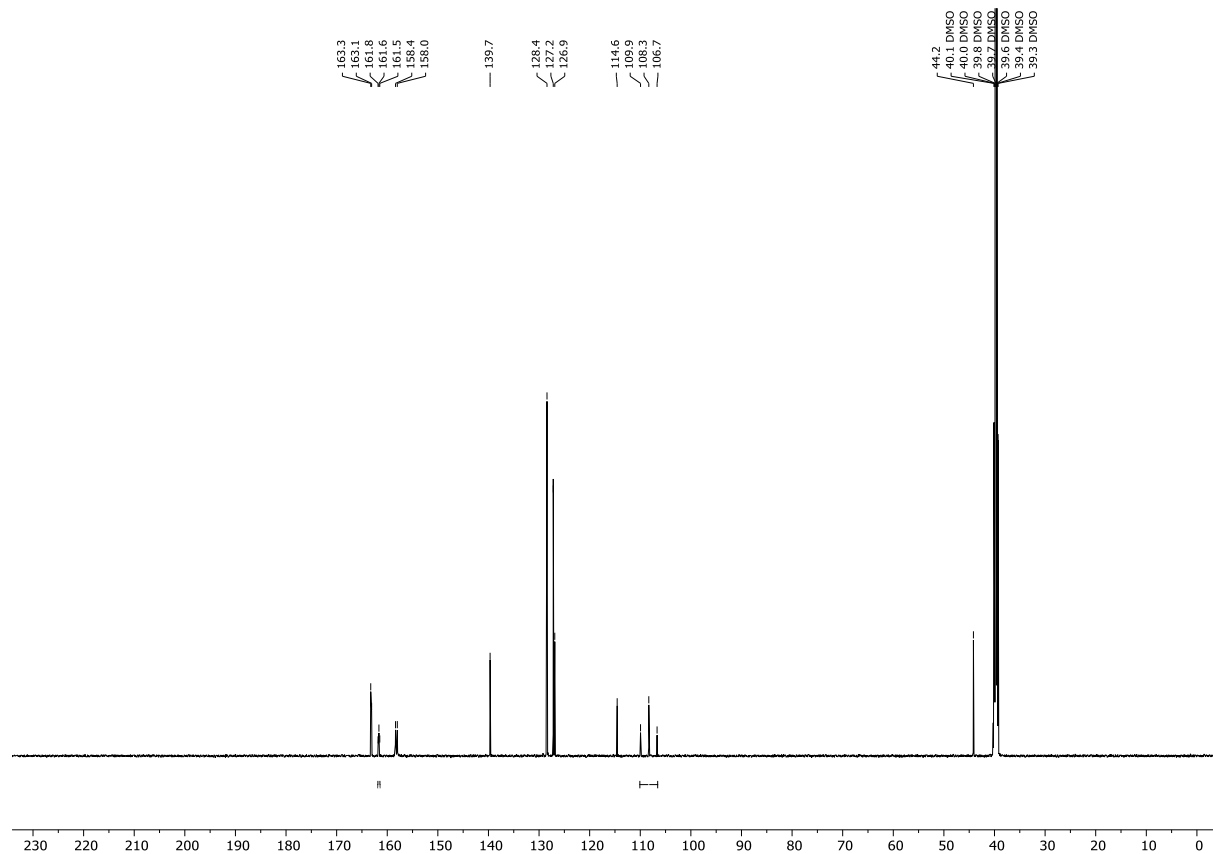
^{19}F NMR spectrum of **12 (565 MHz, $\text{DMSO-}d_6$)**



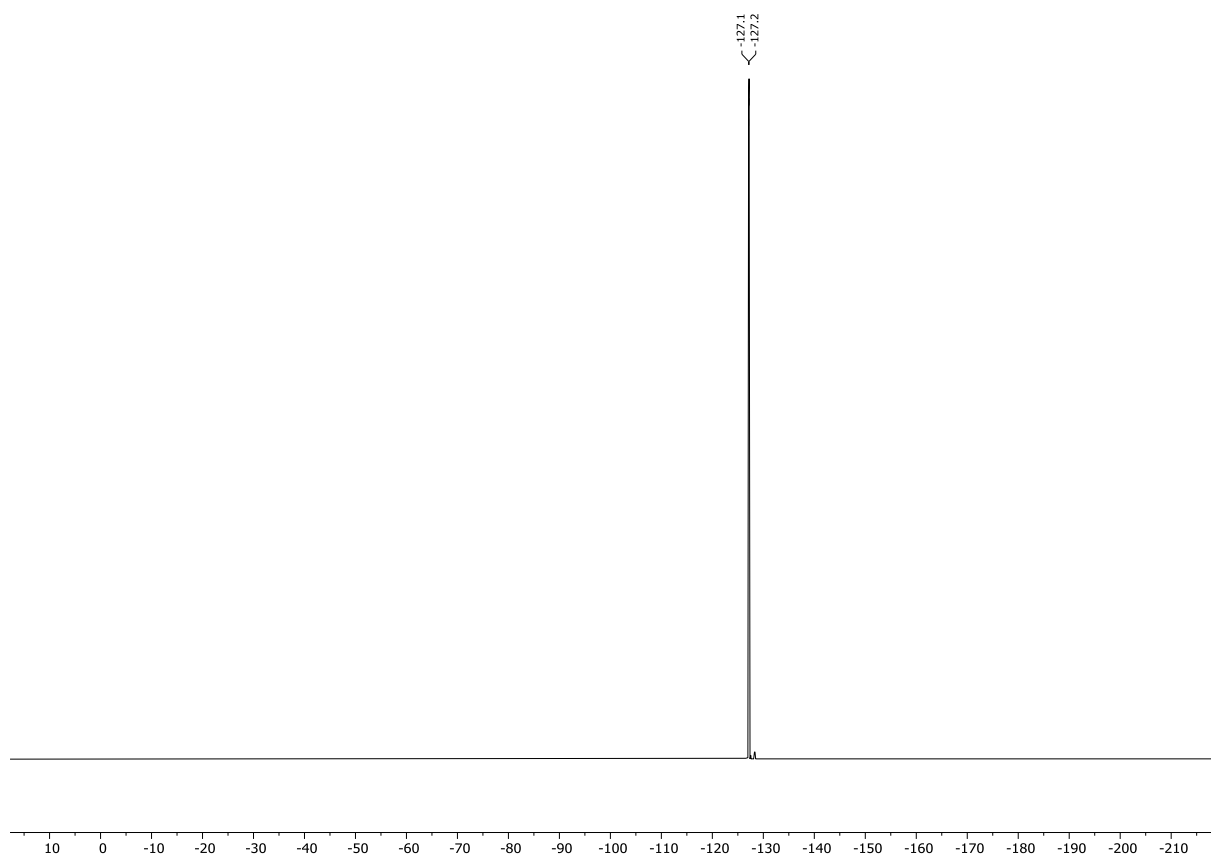
¹H NMR spectrum of 13 (600 MHz, DMSO-*d*₆)



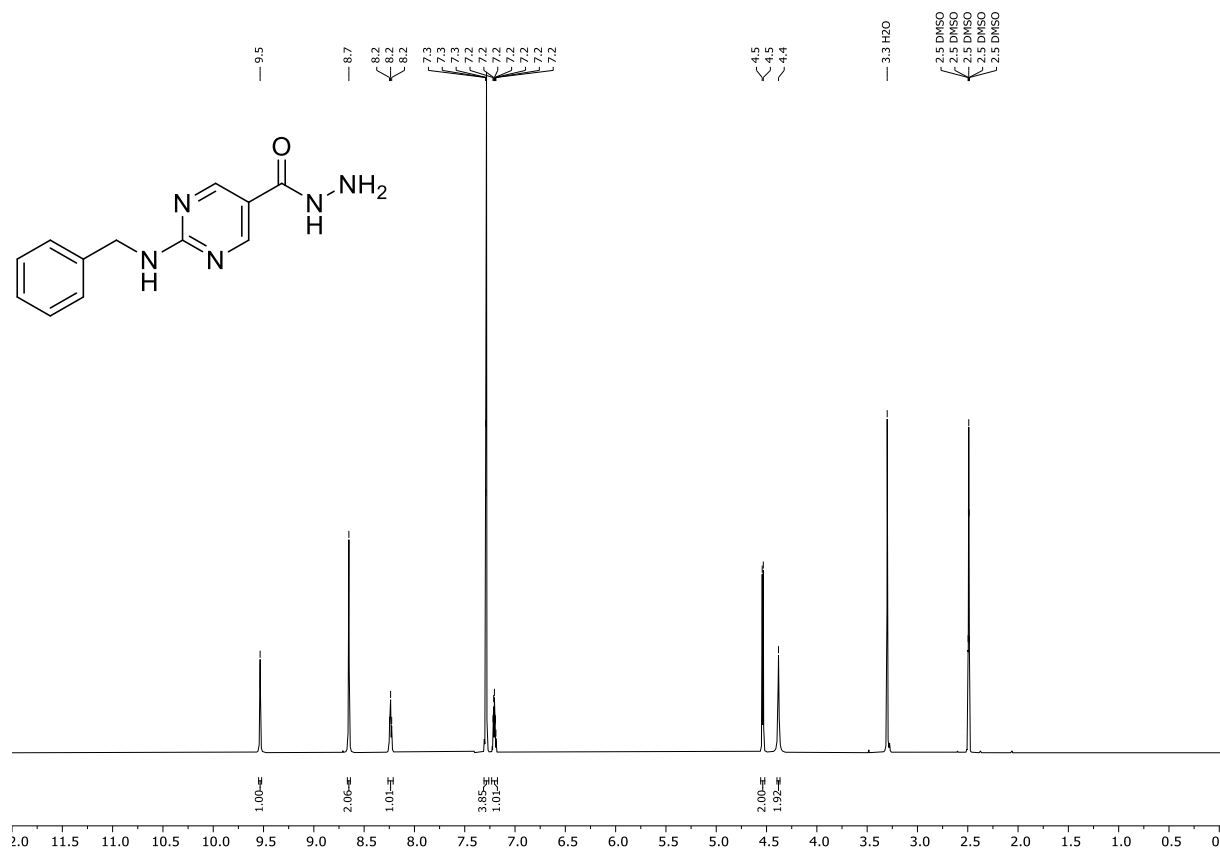
¹³C NMR spectrum of 13 (151 MHz, DMSO-*d*₆)



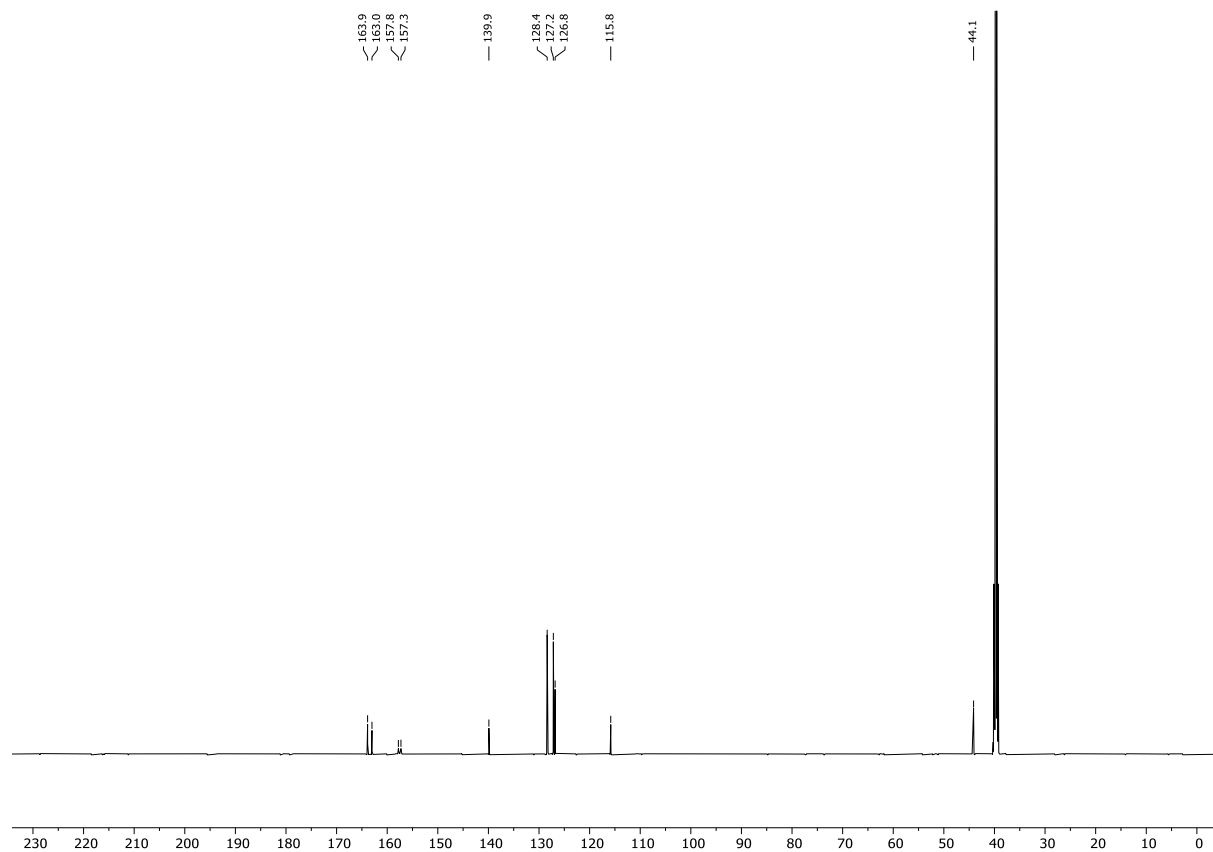
^{19}F NMR spectrum of **13 (565 MHz, $\text{DMSO-}d_6$)**



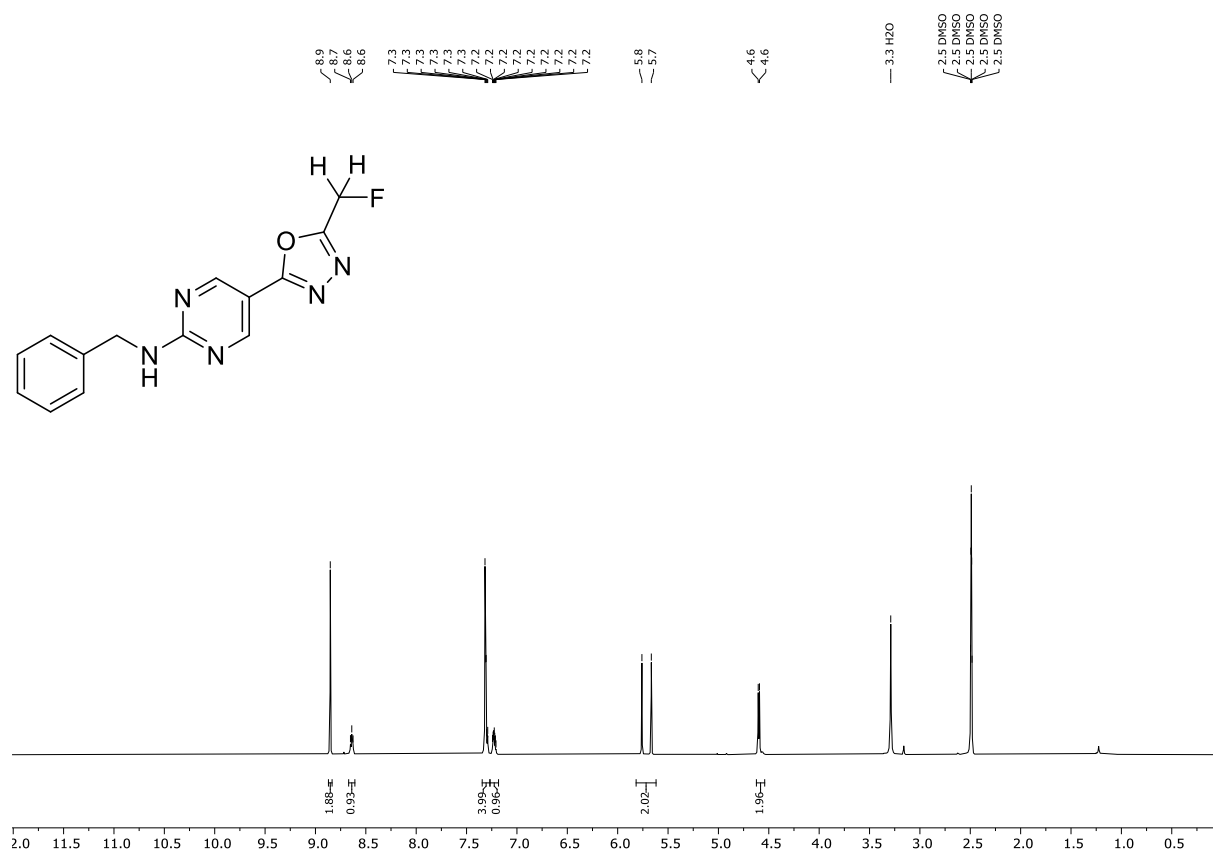
¹H NMR spectrum of 14 (600 MHz, DMSO-*d*₆)



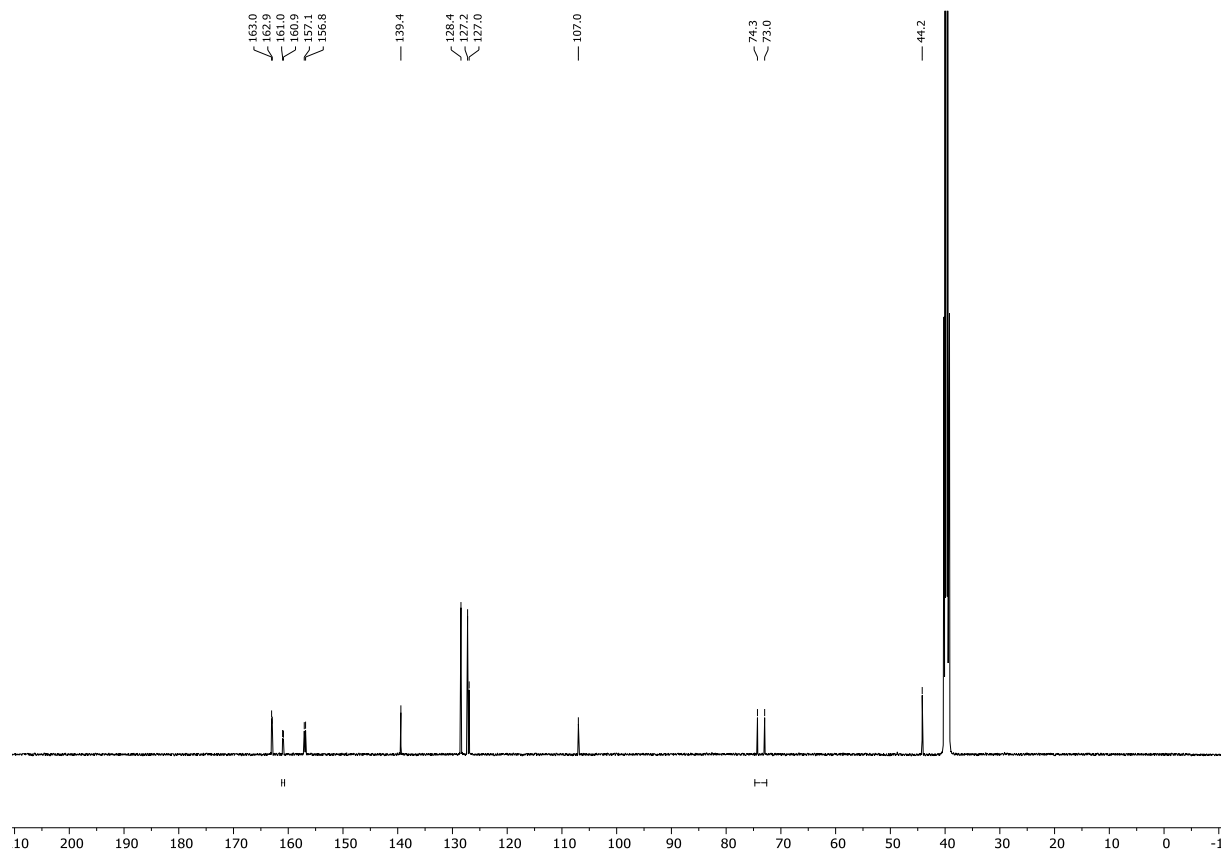
¹³C NMR spectrum of 14 (151 MHz, DMSO-*d*₆)



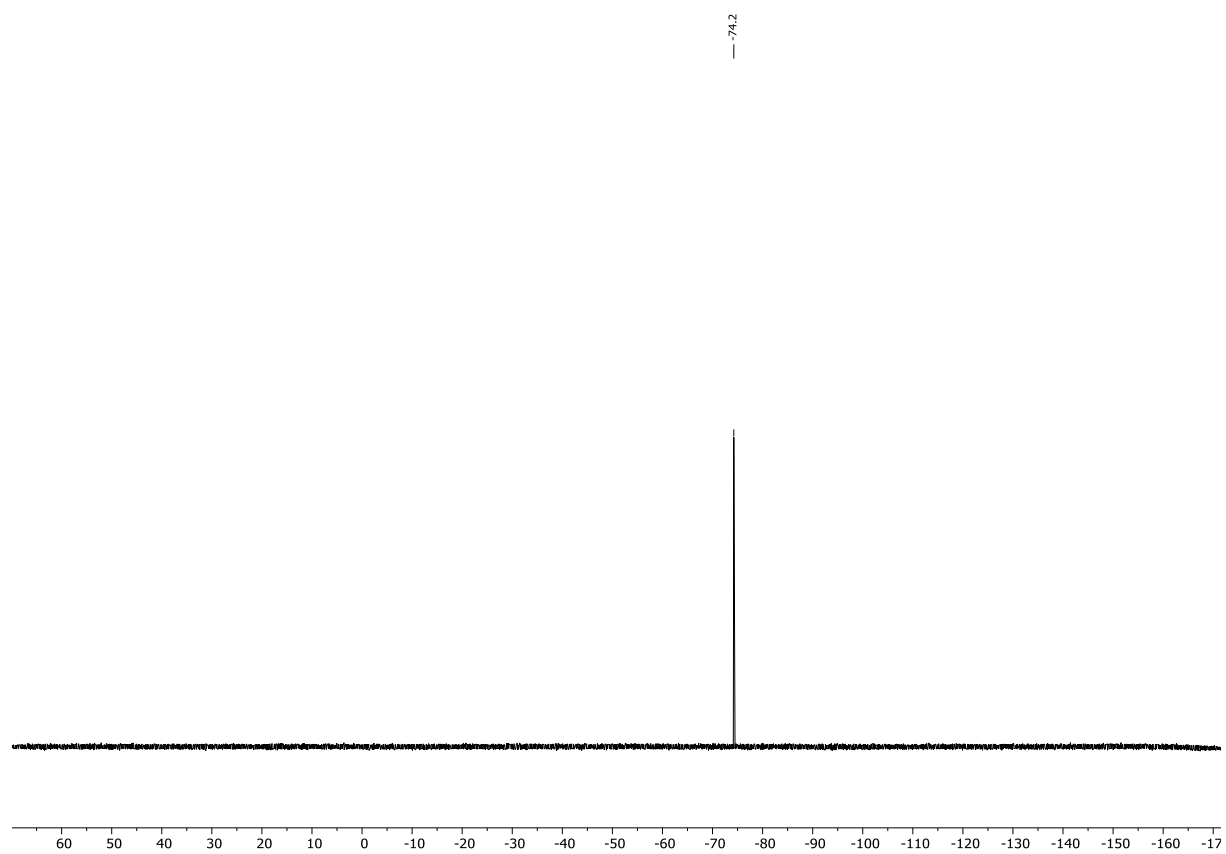
¹H NMR spectrum of 16 (500 MHz, DMSO-*d*₆)



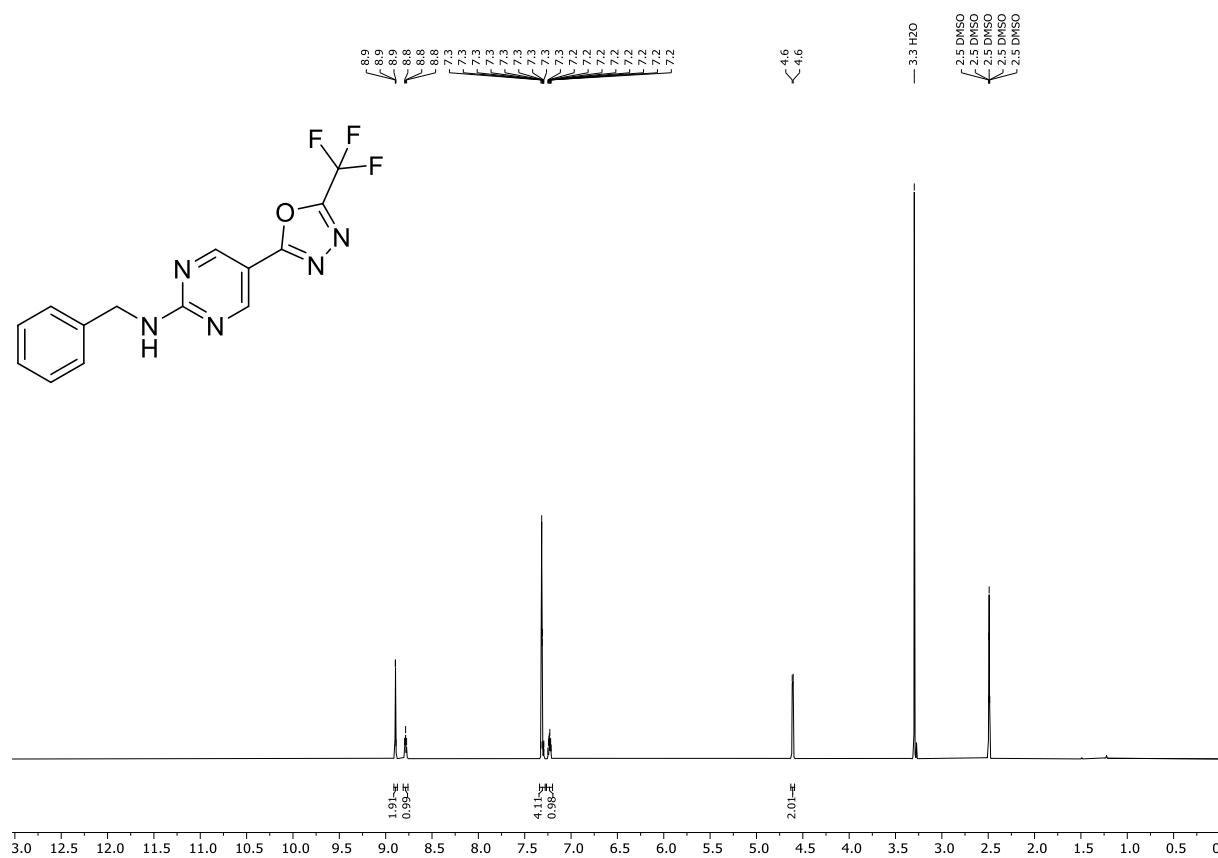
¹³C NMR spectrum of 16 (126 MHz, DMSO-*d*₆)



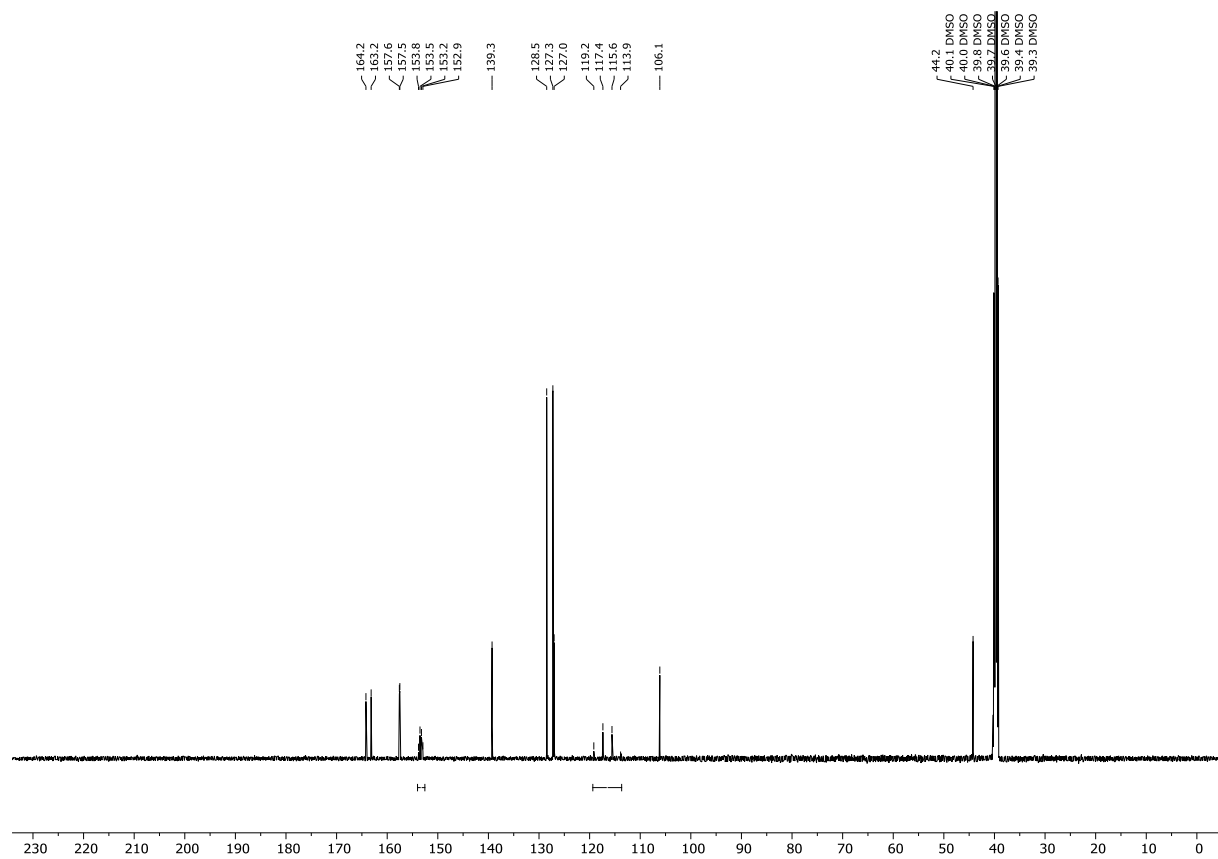
^{19}F NMR spectrum of **16** (471 MHz, $\text{DMSO-}d_6$)



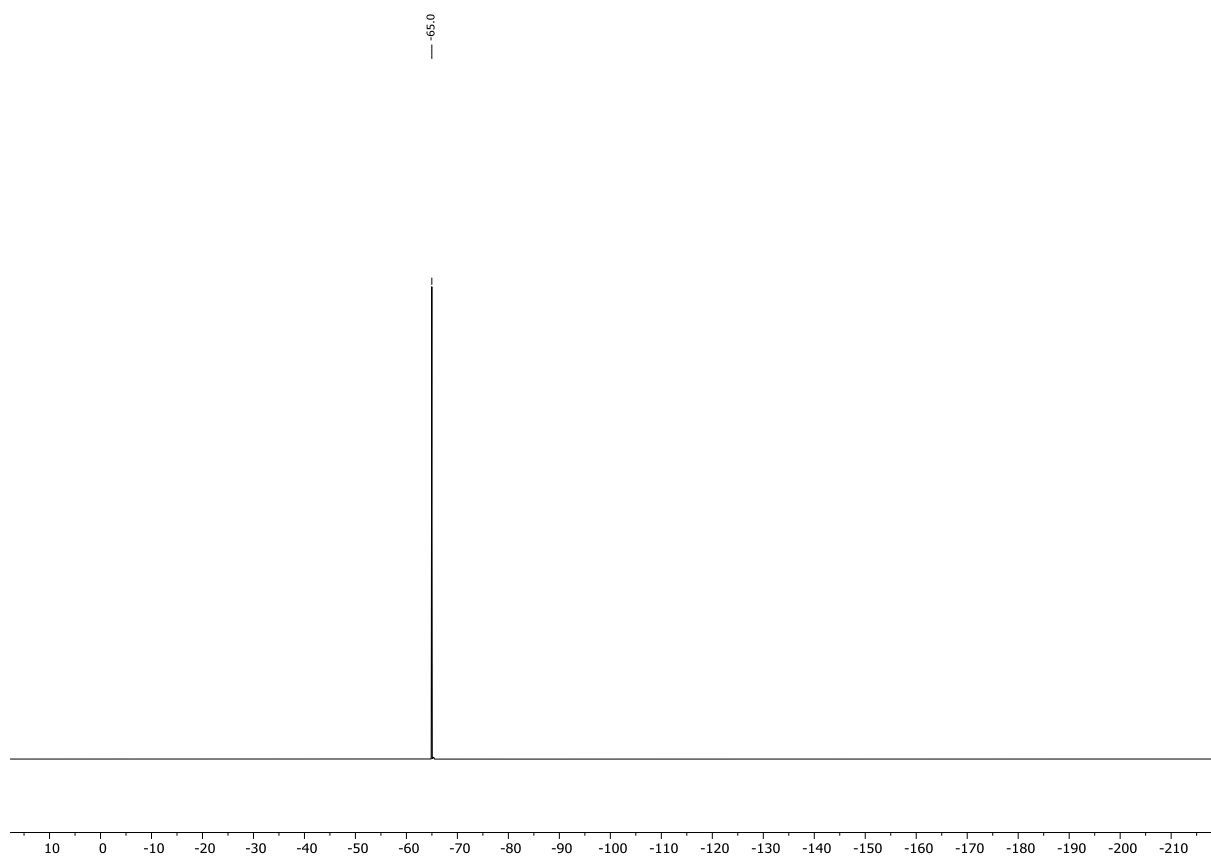
¹H NMR spectrum of 17 (600 MHz, DMSO-d₆)



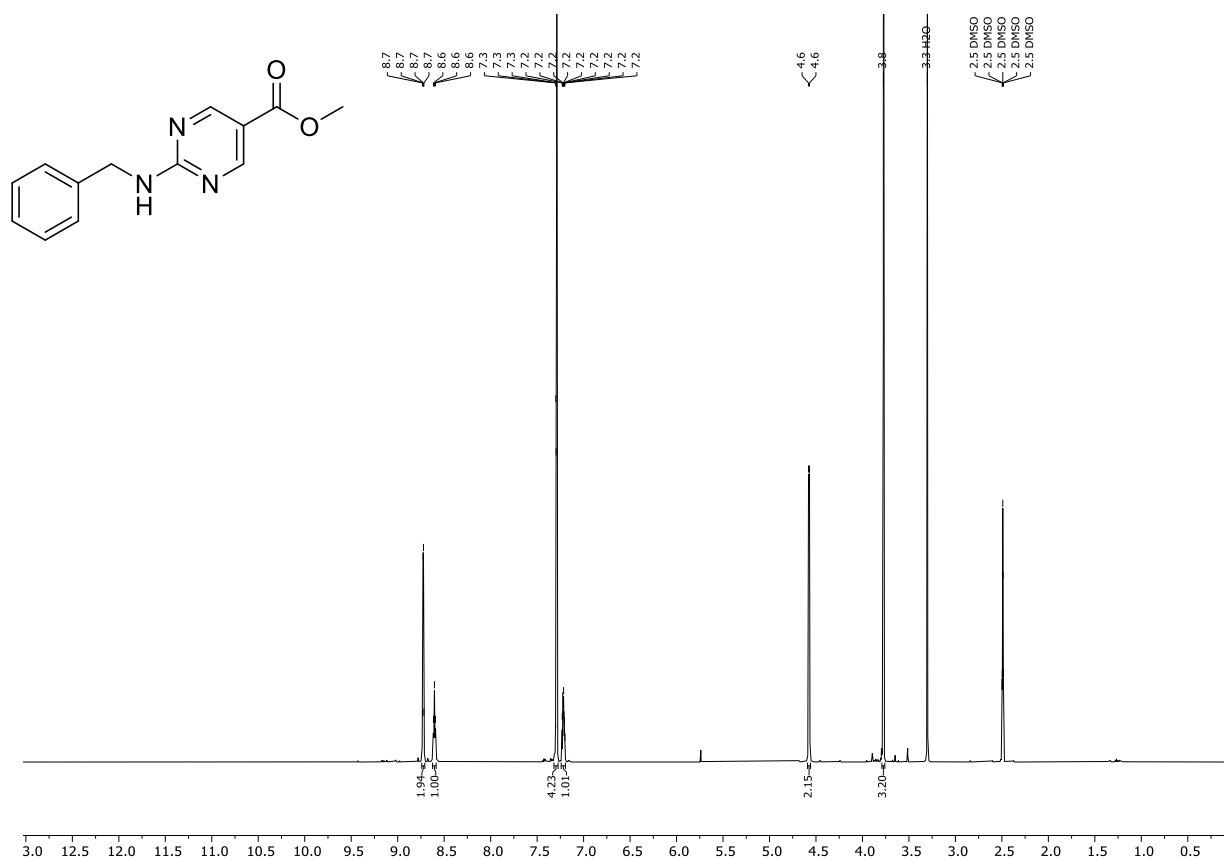
¹³C NMR spectrum of 17 (151 MHz, DMSO-d₆)



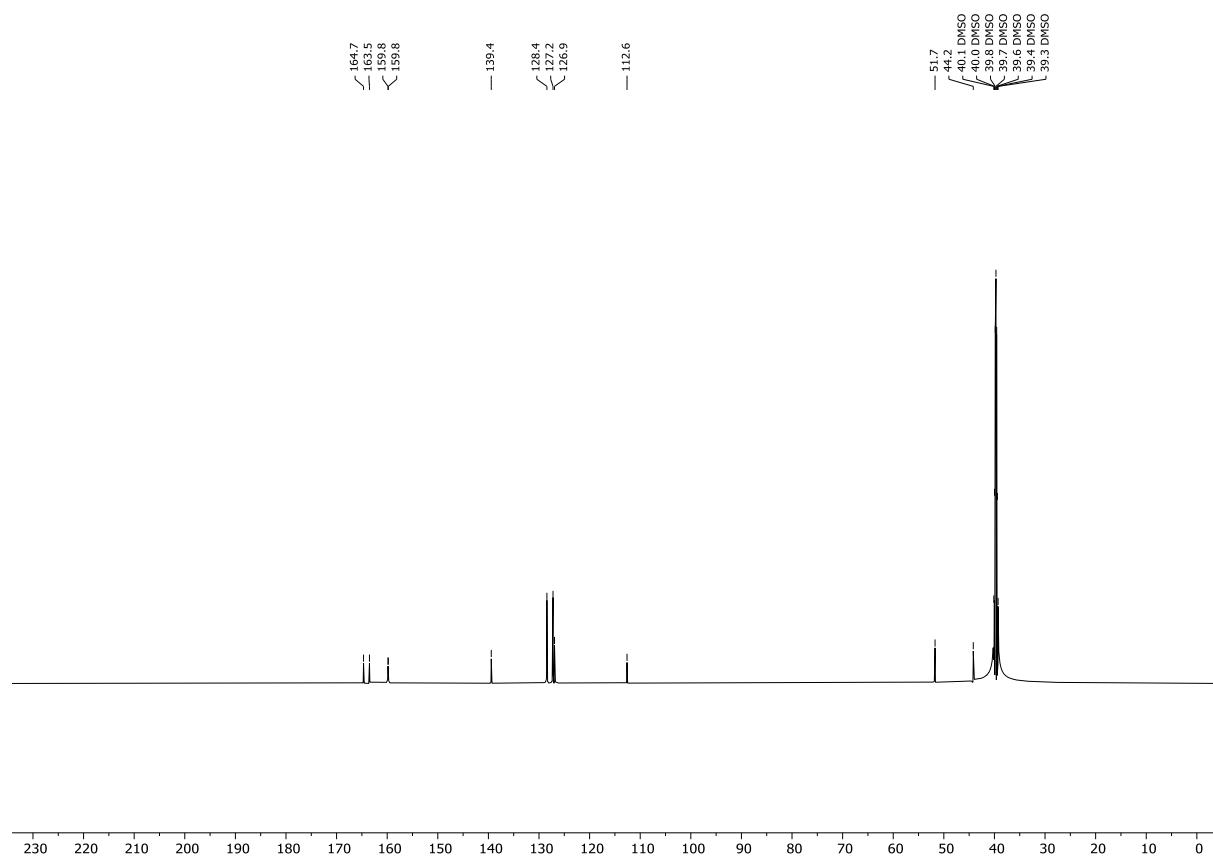
^{19}F NMR spectrum of **17** (565 MHz, $\text{DMSO-}d_6$)



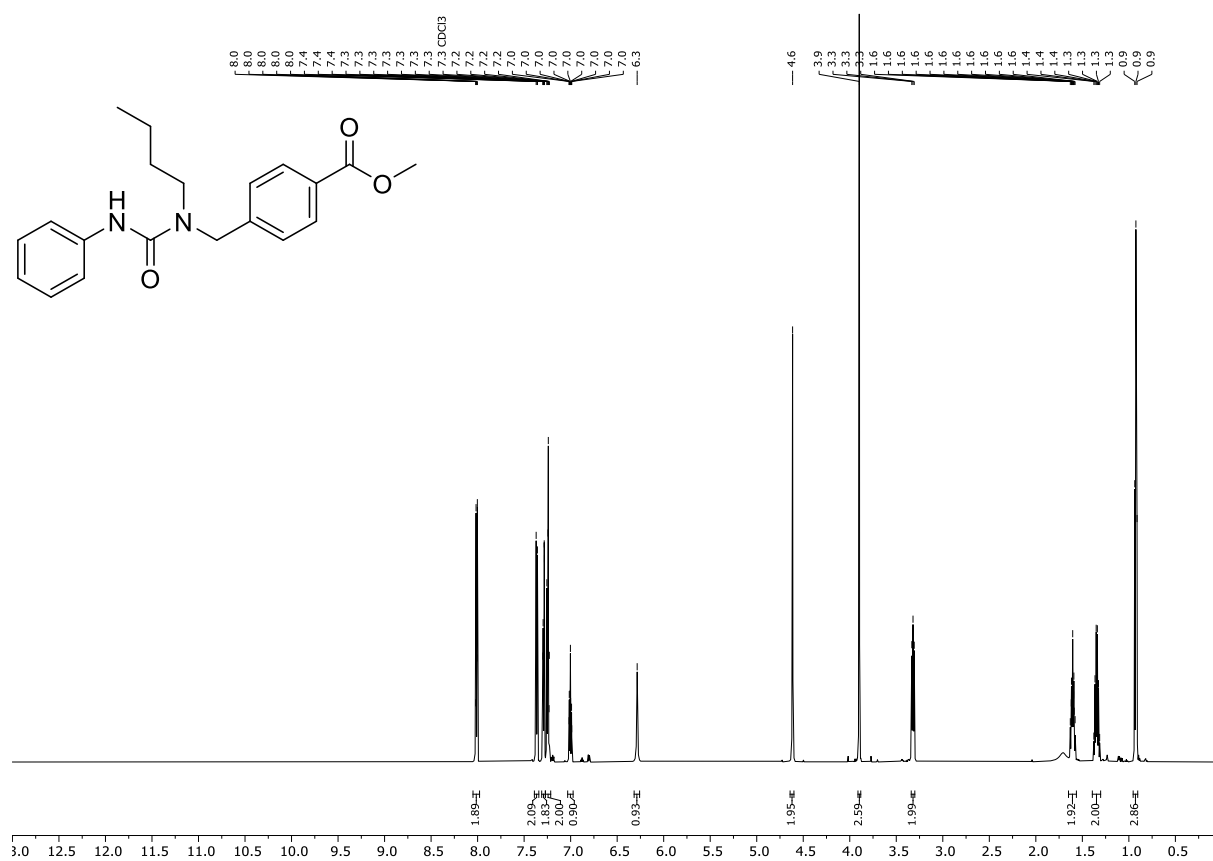
¹H NMR spectrum of 18 (600 MHz, DMSO-*d*₆)



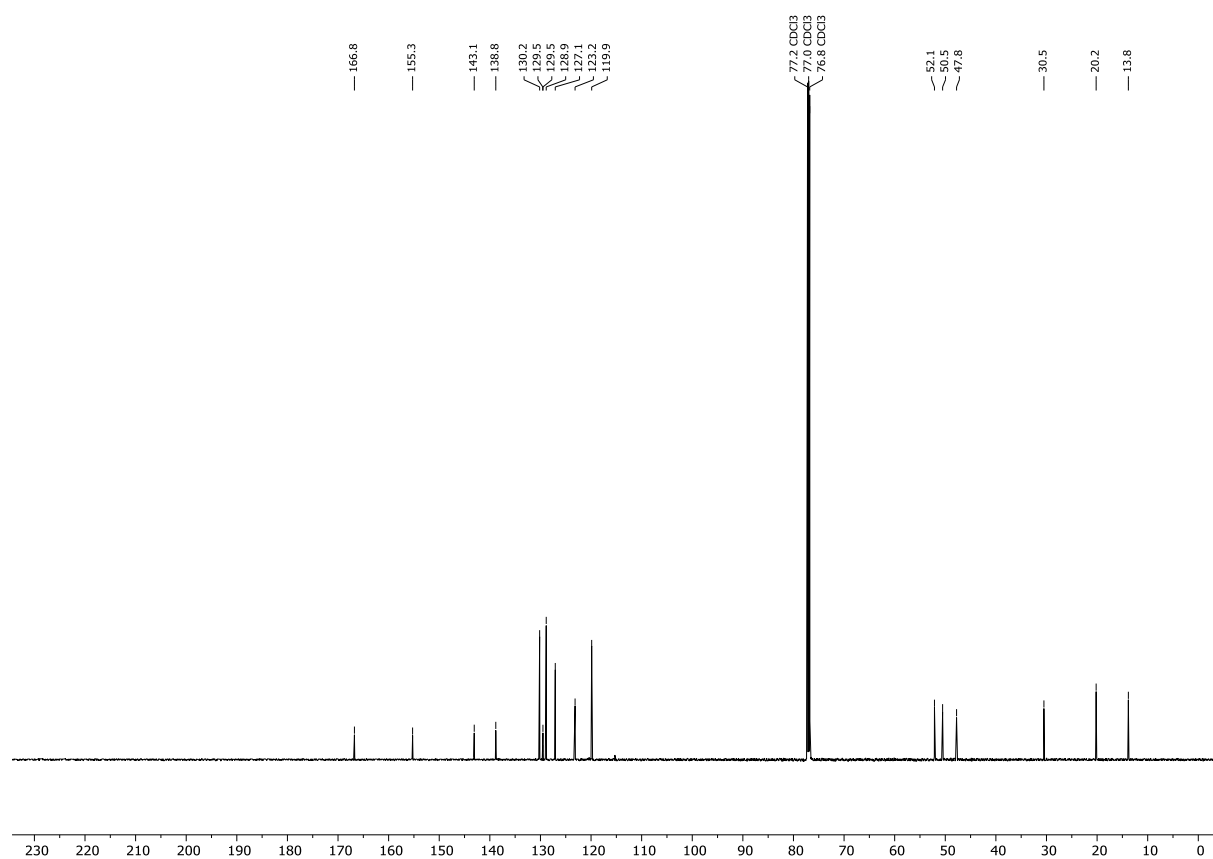
¹³C NMR spectrum of 18 (151 MHz, DMSO-*d*₆)



¹H NMR spectrum of 19 (600 MHz, CDCl₃)

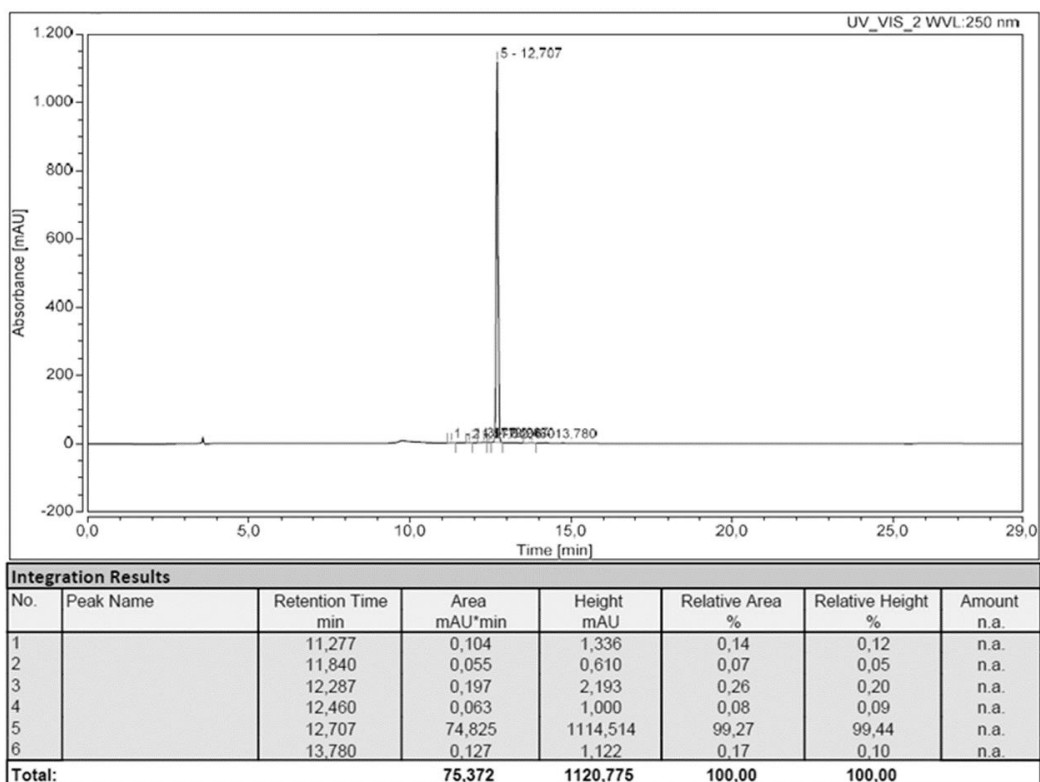


¹³C NMR spectrum of 19 (151 MHz, CDCl₃)

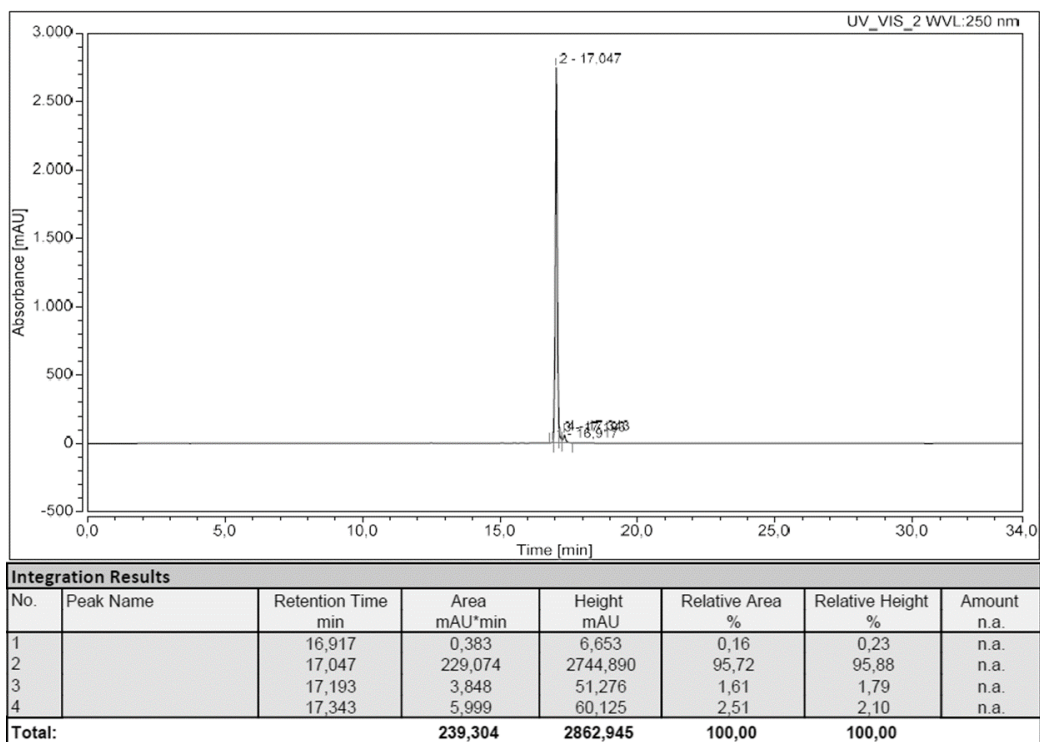


3 HPLC Chromatograms

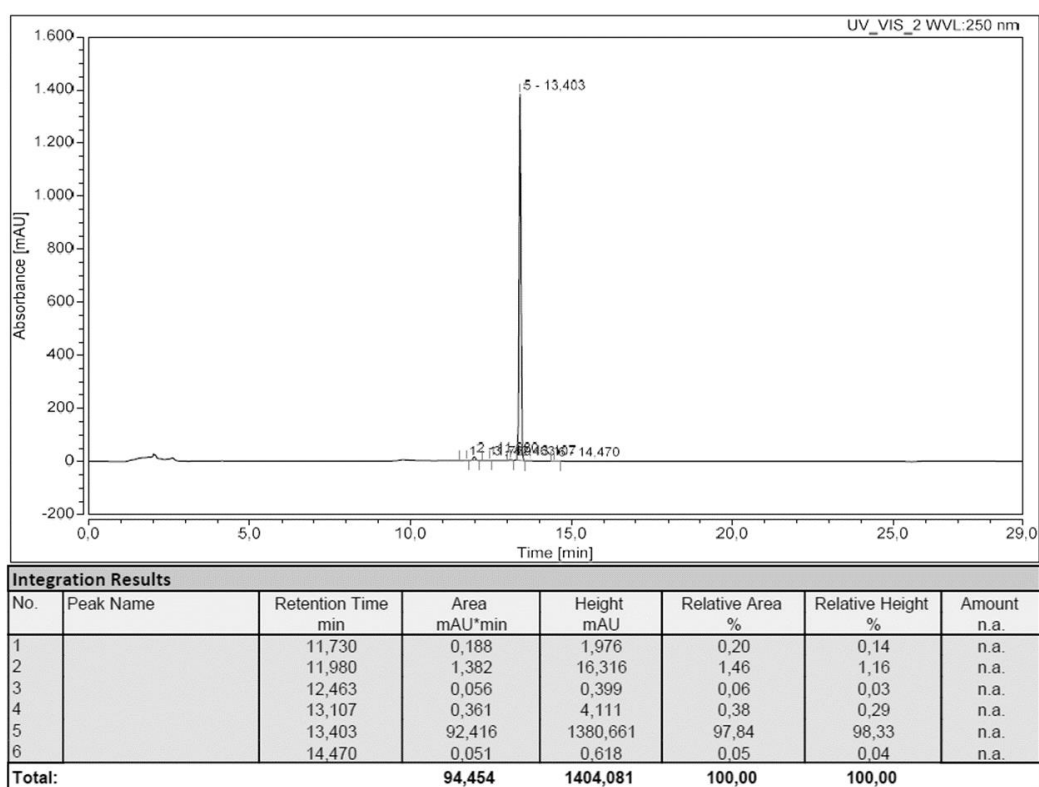
HPLC chromatogram of **6**.



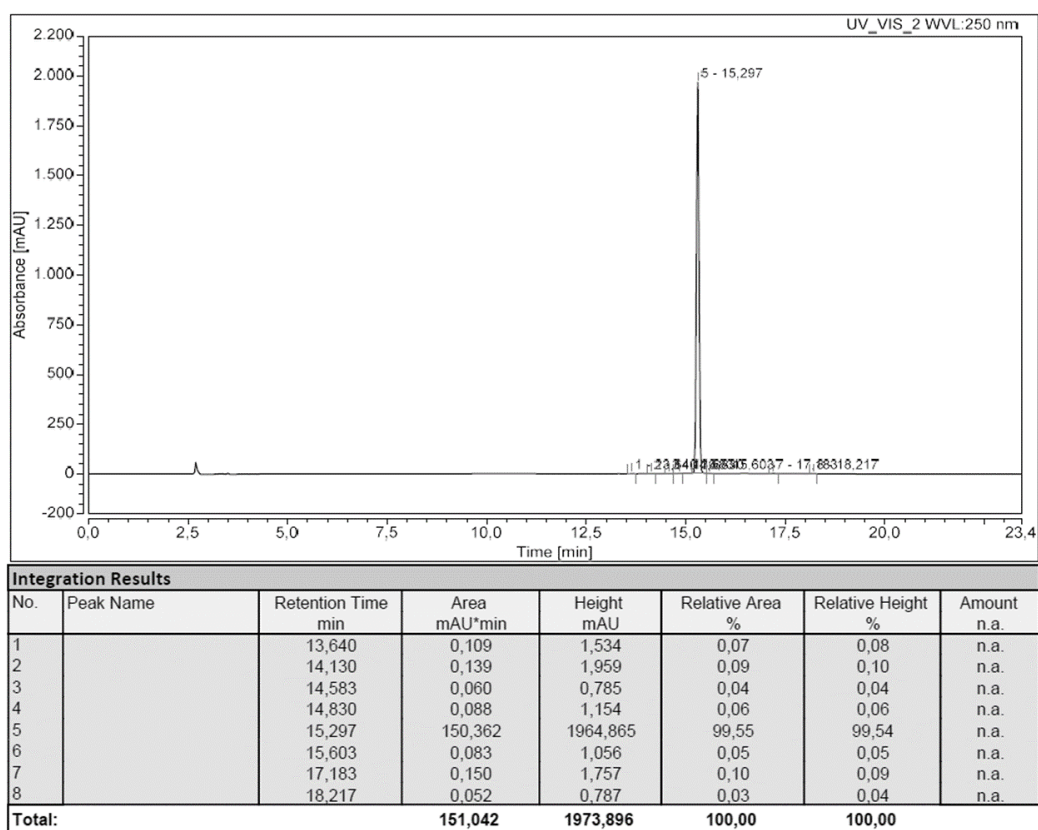
HPLC chromatogram of **9**.



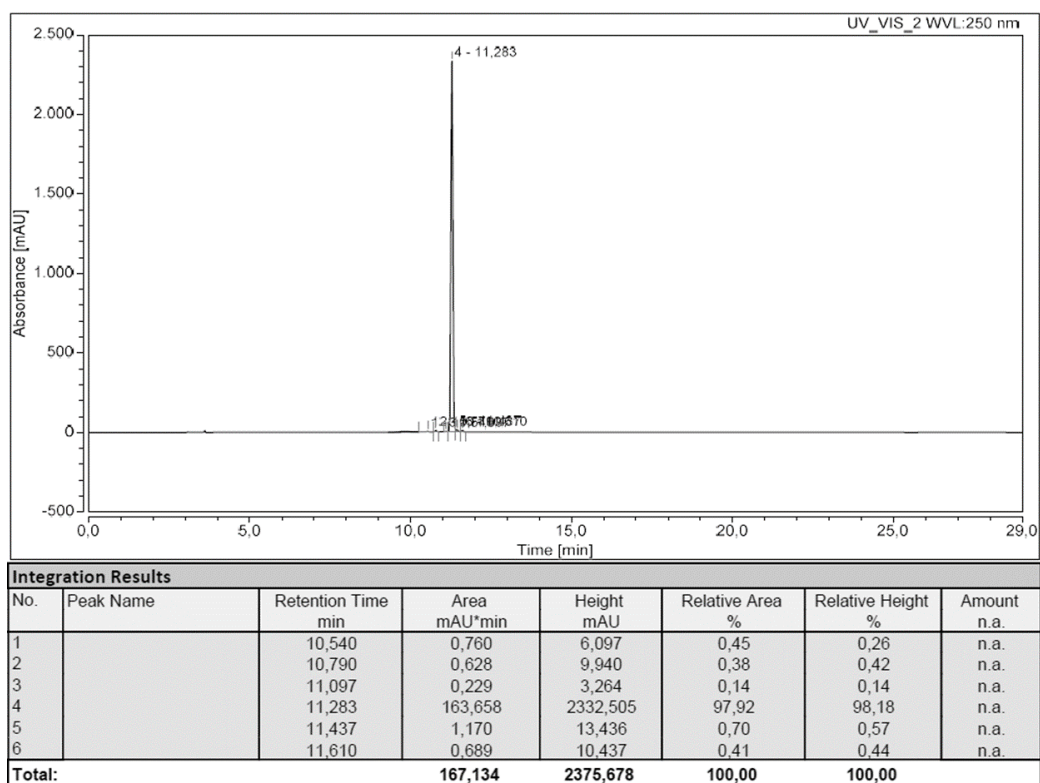
HPLC chromatogram of 10.



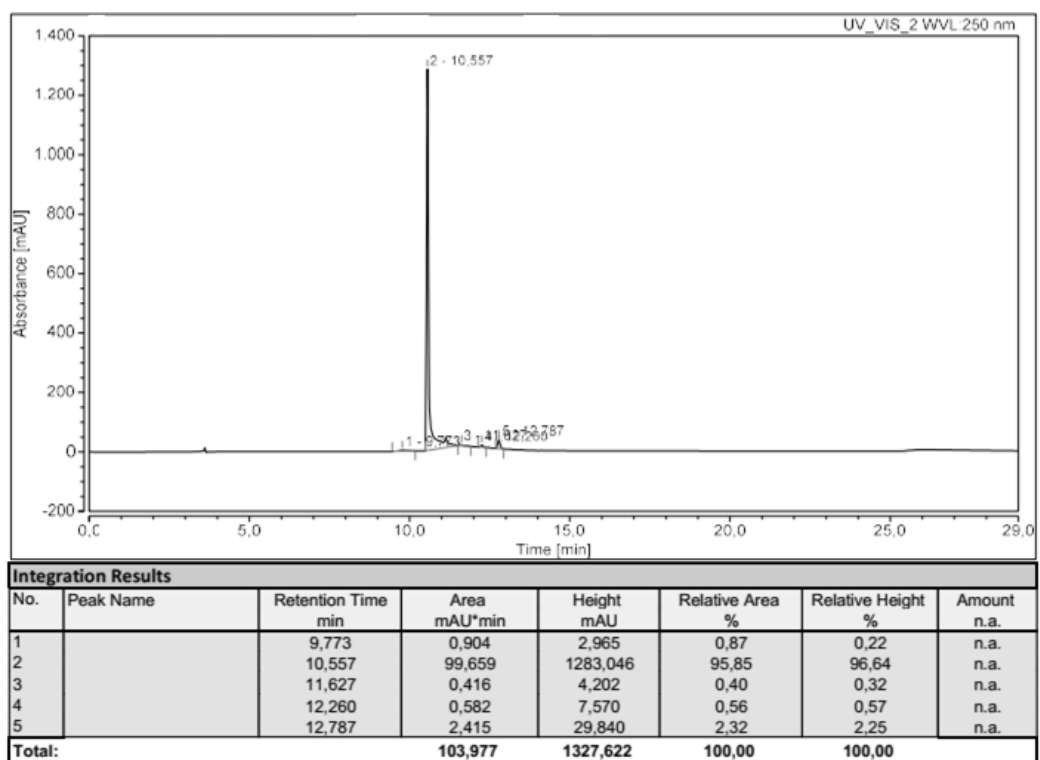
HPLC chromatogram of 12.



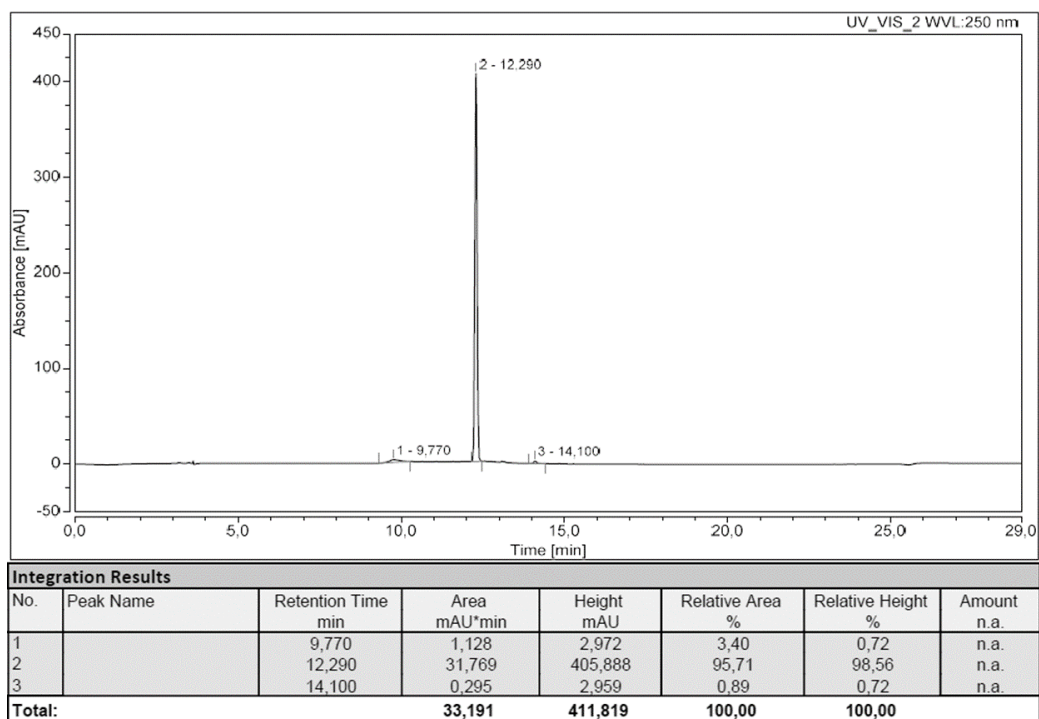
HPLC chromatogram of 13.



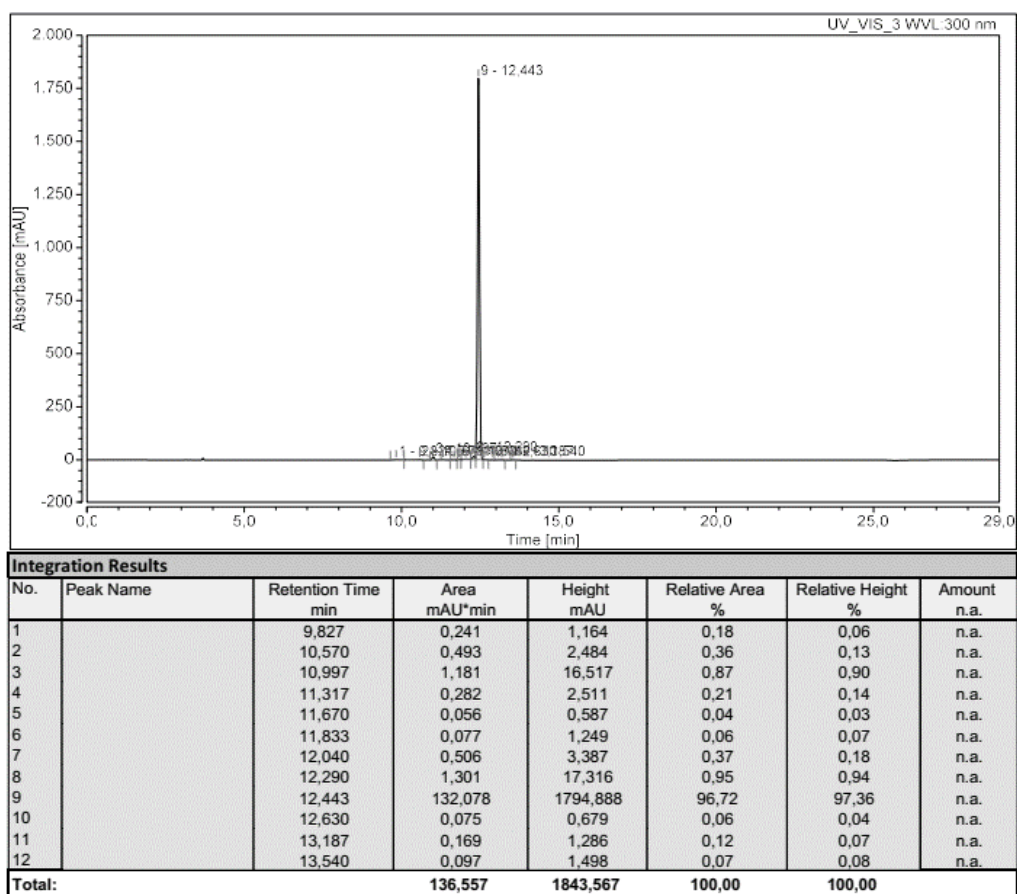
HPLC chromatogram of 14.



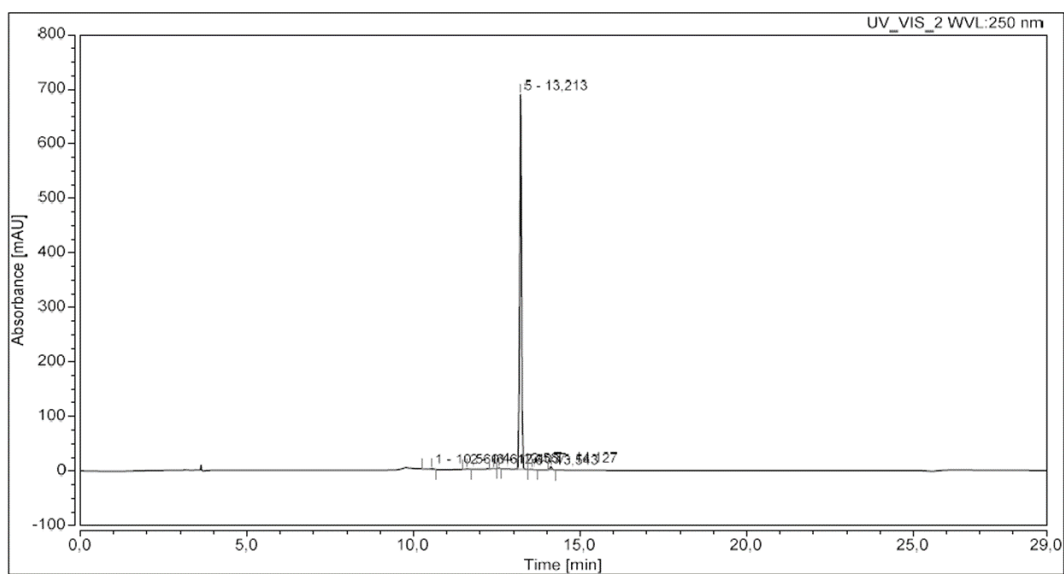
HPLC chromatogram of 15.



HPLC chromatogram of 16.



HPLC chromatogram of 17.



Integration Results							
No.	Peak Name	Retention Time min	Area mAU*min	Height mAU	Relative Area %	Relative Height %	Amount n.a.
1		10,560	0,283	2,011	0,63	0,29	n.a.
2		11,617	0,096	1,234	0,21	0,18	n.a.
3		12,403	0,079	0,833	0,18	0,12	n.a.
4		12,567	0,149	2,399	0,33	0,34	n.a.
5		13,213	43,425	687,496	97,30	97,94	n.a.
6		13,543	0,125	1,441	0,28	0,21	n.a.
7		14,127	0,473	6,510	1,06	0,93	n.a.
Total:			44,629	701,925	100,00	100,00	

4 References

- (1) Yung-Chi, C.; Prusoff, W. H. Relationship between the Inhibition Constant (KI) and the Concentration of Inhibitor which causes 50 per cent Inhibition (I50) of an Enzymatic Reaction. *Biochem. Pharmacol.* **1973**, *22*, 3099–3108.
- (2) Schäker-Hübner, L.; Haschemi, R.; Büch, T.; Kraft, F. B.; Brumme, B.; Schöler, A.; Jenke, R.; Meiler, J.; Aigner, A.; Bendas, G.; Hansen, F. K. Balancing Histone Deacetylase (HDAC) Inhibition and Drug-Likeness: Biological and Physicochemical Evaluation of Class I Selective HDAC Inhibitors. *ChemMedChem* **2022**, *17*, e202100755.